Synthesis of nanomaterials by electrode erosion using discharges in liquids

Anna V. Nominé, Thomas Gries, Cédric Noel, Alexandre Nominé, Valentin A. Milichko, Thierry Belmonte

Synthesis of nanomaterials by electrode erosion using discharges in liquids

A. V. Nominé[1], Th. Gries[1], C. Noel[1], A. Nominé[1,2], V. Milichko[1,2], T. Belmonte[1,*]

[1] Université de Lorraine, CNRS, IJL, F-54000 Nancy, France

[2] ITMO University, St. Petersburg 197101, Russia

* corresponding author. Email: thierry.belmonte@univ-lorraine.fr

PACS number: 52.80.Wq Discharge in liquids and solids

Keywords: Spark discharges; Submerged discharges; Time-resolved optical emission spectroscopy; Liquid nitrogen.

ABSTRACT

Discharges in liquids are very efficient to synthesize nanoparticles by electrode erosion. This simple process is only simple in appearance. Mechanisms responsible for the production of nanoparticles are several, depending on the choice of process parameters. They determine size distributions, shapes, composition and defects of produced particles. They also control their possible assembly into more complex structures. This paper describes the basic physics of nanoparticles synthesis by discharges in liquids using electrodes and gives a summary of the research efforts that have been devoted to the understanding of this process. A special attention is paid to thermodynamics of these systems driven by discharges that are at or close to local equilibrium. Although a complete picture is not available yet, huge progress has been made and offers new capabilities for a better control of this kind of processes. Finally, among important challenges that are still to tackle, the possibility of forming nanoalloys from immiscible elements or achieving unimodal monodisperse size distributions is questioned from the current mastery reached in this field.

I. A BRIEF HISTORY

Discharge-liquid interactions were studied for the first time by Fizeau and Foucault in 1844.[1] They reported light emission from an electrode immersed into an electro-conductive medium. The use of discharges in contact with liquids dates back to 1887, when Gubkin[2] used a glow-discharge cathode to reduce silver ions (Ag^+) in an aqueous solution of $AgNO_3$. This was the beginning of "glow discharge electrolysis" (GDE),[3] as it will be named tens of years later. Other seminal works in this vein followed.[4,5] Discharges in liquids were intensively studied at the end of the XIX century, when researchers wanted

to clarify breakdown mechanisms in these media,[6] an undertaking that is still running. Discharge-assisted electrochemistry inspired biologists who dreamt of creating conditions favourable to the emergence of life thanks to these non-faradic electrochemical reactions.[7]

In the middle of the twentieth century, the so-called "electrode effect", *i.e.* the glow discharge taking place at either electrode depending on the voltage polarity, originally observed in molten salts, was also observed in aqueous solutions.[8] Hickling and Newns[3] discovered that the chemical performances of the GDE processes were several times the values of Faraday's law of electrolysis. The chemical products were different from those of conventional electrolysis such as the release of large amounts of molecular hydrogen and hydrogen peroxide, as well as the H· and OH· radicals in the liquid phase, among other secondary reactions products.[9,10]

Very early, erosion of submerged electrodes was noticed. Joseph Priestly described the phenomenon of material erosion by electric spark in 1878.[11] But it is only in 1930 that he patented the idea to exploit it for electrical discharge machining (EDM).[12] This process is among the earliest non-traditional manufacturing processes.[13] Material removal by controlled erosion through a series of sparks was actually developed in the USSR during the 1940s. B.R. and N.I. Lazarenko first applied it to a machine for stock removal.[14] Full commercial exploitation started only in the 1960s. The production of particles by EDM was considered as a drawback, making the process drift. Powdery by-products were simply not considered as a potential subject of study.

Nairne was the first to make silver and copper wires explode in 1774.[15] Apparently, the production of ultrafine powders by the exploding wire technique was begun by Abrams,[16] who studied radioactive Al, U, and Pu aerosols. In this process, the breakage of the wire in the liquid state leads to the disintegration of the wire in the form of hot microdrops or clusters.[17] Joncich and Reu in 1964 chose to make explosions in liquid nitrogen to produce metal nitrides particles.[18] The wires are most often placed in water.[19,20] This allows one to increase the energy deposition and to use the converging shock wave generated by the exploding wire array to reach high pressure on the axis of the implosion.[21] The production of nanoparticles by this process is still the subject of active research.[20,22,23] Explosions in general imply the presence of a plasma phase and a liquid phase.

By comparing the explosive detonation parameters with the carbon phase diagram and performing thermodynamic calculations, it has been shown empirically and theoretically that free carbon in detonation products of powerful condensed carbon-containing individual explosives with a negative oxygen balance should condense in a diamond or liquid phase.[24] This applies to the synthesis of nanodiamonds discovered first in the USSR in 1963 by Volkov, Danilenko and Elin.[25]

The situation changed dramatically with the advent of laser-based processes. Maiman constructed in 1960 the first functional pulsed-laser using a ruby crystal and emitting at 694 nm,[26] enabling the development of pulse laser ablation shortly afterwards by Smith and Turner.[27] Patil *et al.*[28] introduced

the concept of pulsed laser ablation at the solid-liquid interface in 1987. This method, known as Liquid Phase Pulsed Laser Ablation (LP-PLA), Laser Ablation in Liquids (LAL) or Laser Ablation Synthesis in Solution (LASiS), is based on the erosion of a solid target immersed in a solution by a laser beam focused through the liquid onto the solid surface. Progress in laser technology led to ultrashort pulse lasers (*i.e.* picosecond in 1964,[29,30] and femtosecond in 1981,[31]), which brought considerable perspectives to ablation in liquids by affecting basically the mechanisms of the erosion of solids.[32] Moreover, accessing to synthesis conditions that are far from thermodynamic equilibrium opened up new possibilities, among which the synthesis of nanomaterials with original properties.[33]

The idea of using discharges to create conditions for such a purpose made submerged discharges a possible alternative to lasers as sources of energy deposition. The first works mentioning the synthesis of "fine powders" by discharges in liquids were published by Ishibashi *et al*.[34] They proposed a spark discharge method, in which a spark discharge takes place at the contact points of pellets dipped in the liquid medium. There is no doubt that nanoparticles were also synthesized in these conditions. Dubovoy *et al.*[35] proposed a similar approach in 1985 as well as Sato *et al.*[36] in 1992. The first experiments mentioning the synthesis of nanomaterials were certainly carried out by Ishigami *et al.*[37] in the USA who wanted to propose a simplified synthesis method of carbon nanotubes by arc discharges. This strategy eliminates nearly all of the complex and expensive machinery associated with conventional nanotube growth techniques. Sano *et al.*[38] in the UK demonstrated one year later with a similar device the possibility of producing carbon onions. The topic starts taking off in 2004, likely because of the ease of running these processes. The idea of resorting to ultrasound assistance came up quickly[39] as it was studied to improve the material removal rate, to reduce the tool wear rate and to optimise the surface quality of the machined workpieces in EDM.[40,41]

The idea of locating the plasma outside the discharge came back in 2005 with an alternating current (AC) plasma source.[42] Two years before, generation of nanomaterials by melting and evaporation of a sacrificial metal electrode in a microplasma was demonstrated for the first time by Shimizu *et al.*[43]. Next, other solutions of GDE-type processes were proposed.[44–46] Corona discharges usually employed in GDE were replaced by various atmospheric plasmas among which Dielectric Barrier Discharges.[47] The concept was applied to surface functionalization of nanoparticles by Mariotti *et al.*[48]

The formation of bubbles (or their pre-existence) in liquids, submitted to an injection current, was the most studied mechanism responsible for breakdown. The formation of pre-breakdown bubbles was examined in the 60s. [49,50] Discharges in bubbles injected on purpose in a liquid became a new process as such when Yamabe *et al.* proposed this concept in 1993.[51] Their utilization for nanoparticles synthesis was proposed only very recently. Shin *et al.*[52] produced carbon nanomaterials by discharges in Ar/O_2 gas bubbles injected in 1-hexanol and by Yamada *et al.* who used a gas–liquid slug flow reactor system.[53]

A bubble in a liquid can be considered as the counterpart of a droplet in a gas. Both are submitted to discharge-liquid interactions in the processes we are interested in. This is especially the case of warm dense matter produced for instance by ultra-intense laser excitation of liquid fuel targets,[54] a domain far beyond the scope of this paper. The technological importance of introducing droplets in discharges was first foreseen at the end of the 19th century by Schoop in Switzerland. He used flames to coat metal surfaces with lead and tin,[55,56] inventing plasma spray. The process was strongly improved in the 50s with the development of plasmatron systems.[57] Droplets in cold plasmas were studied much later because studies were for long devoted to the sole interaction between electric fields and droplets in neutral gas, after the discovery by Taylor in 1964 of a condition for stable liquid cone existence.[58] Hager and Dovichi studied the behaviour of microscopic liquid droplets near a strong electrostatic field and developed the droplet electrospray.[59] The repulsion was a result of droplet charging via the corona discharge created at the tip of the high-voltage probe. In a related study, Kim and Dunn investigated the formation of progeny droplets ejected from a parent droplet, in the presence of an intense electric field.[60] However, investigation of the behaviour of droplets in cold non-equilibrium discharges is much recent. The interest of using pulsed discharge to improve combustion in engines required to investigate this topic.[61,62] Ward *et al.*[63] used an ultrasonic nozzle to atomize acrylic acid monomer into an atmospheric pressure glow discharge (APGD) to deposit polymeric coatings, opening up the way to several other processes alike.[64–66]

Aggregation in low-pressure activated vapour phases leads to ultra-small nanoparticles that can be collected in liquids with extremely low vapour pressure, like oils or ionic liquids, which enables the production of nanofluids. The vapour phase can be created by any physical source like evaporation[67] or sputtering.[68] The liquid can also be directly decomposed by an electron beam for instance.[69]

We shall not forget to mention that liquid droplets in discharges are also of primary importance for climatologists[70] and astrophysicists.[71] For example, the atmosphere of Titan is constantly bombarded by galactic cosmic rays and Saturnian magnetospheric electrons causing the formation of free electrons and primary ions, which are then stabilized by ion cluster formation and charging of aerosols. These charged particles accumulate in drops in cloud regions of the troposphere.

The synthesis of nanoparticles by discharge-liquid interactions involves the presence of all states of matter. The previous history, because it is intentionally short, is biased to select some seminal works as breakthroughs in the topic. The following paper is centred on nanoparticles synthesis. Other correlated aspects can be found with much detail in some reference review papers:

- For discharges in liquids, see Refs. 72–83
- For discharges in contact with liquids, see Refs. 48, 84–96
- For laser in liquids, see Refs. 32,33, 97–104
- For spray in discharges, see Refs. 105–110

- For electrical wire explosion, see Refs. 22, 111
- For sputtering onto liquids, see Refs. 112–117

or in books, see Refs. 6, 81, 118-122.

To the best of our knowledge, no review or book is available about nanoparticles synthesis for discharges in bubbles.

II. EXPERIMENTAL APPROACHES

There are two main ways to generate a direct current (DC) discharge in a liquid to synthesise nanoparticles. A low-voltage generator (typically below 1 kV) can be used, which requires to put the two electrodes in contact, the discharge being created when the gap between the electrodes increases, either by material erosion or by mechanical separation. The current[123,124] or the voltage[125] are, most often, used as closed-loop feedback signals to keep the inter-electrode gap distance, measured with a detector, as constant as possible. For instance, Bera *et al.*[126] developed an optoelectronic system made of three main components to maintain constant a preselected distance between the electrodes (**Fig. 1**): a photosensor for an optical emission diagnosis, a feedback loop which is composed of analog electronics and a computing unit, and a servo-unit for axis translation of the anode.

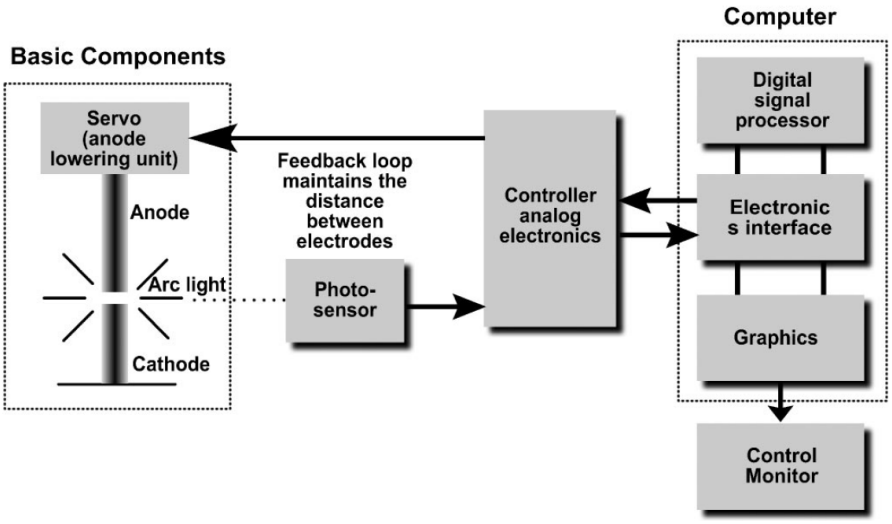

Fig. 1: Block diagram showing the concept and major components of the optoelectronic feedback control of the electrode feeding system that is implemented in the present ADS process. Reproduced from D. Bera, E. Brinley, S. C. Kuiry, M. McCutchen, S. Seal, H. Heinrich and B. Kabes, Rev. Sci. Instrum. **76**, 033903 (2005), with the permission of AIP Publishing (Fig. 3 in Ref. 126).

Resorting to high-voltage discharges (typically beyond 1 kV) enables breakdown at short gaps (*i.e.* from 100 µm to 1 mm typically, depending to the strength of the dielectric liquid). If one electrode is insulating, AC or radiofrequency (RF) excitation can also be used. **Table 1** *(see at the end of the manuscript)* presents selected examples of discharges in liquids for the synthesis of nanoparticles of

simple metals. It is useful to compare conditions and have practical values of parameters. For carbon materials, a thorough review is available.[72]

Experimentally, reactor designs are many (**Fig. 2**), even though it is relatively simple to set up a process, as only a power generator, two electrodes and a vessel containing the liquid are required. Indeed, the power source can be used to generate a DC, AC (low frequency), radio frequency, microwave, unipolar pulsed discharge or bipolar pulsed discharge. The electrodes can be a pin, a plate or even materials granules. The shape of the vessel can be a cylinder or a cone to prevent the drift of particles from the discharge zone. The process can be assisted by ultrasound.[151,152] One electrode can vibrate to facilitate electrical breakdown and mix the treated solution.[153]

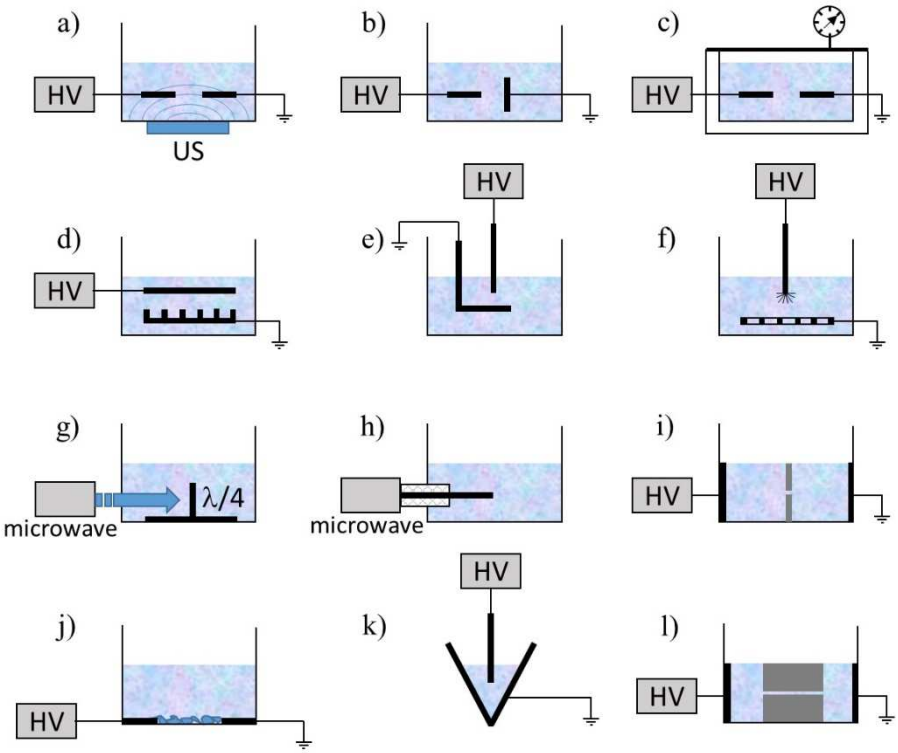

Fig. 2: Selected examples of submerged discharge processes. a) pin-to-pin spark discharge with ultrasound assistance,[152] (b) pin-to-plate,[154] (c) supercritical or cryogenic fluids,[148,155] (d) multi-pin-to-plate,[153] (e) pulsed arc with vibrating electrode,[156] (f) brush-to-plate,[153] (g) microwave discharge with quarter-wavelength antenna,[75] (h) microwave discharge with coaxial line,[75] (i) diaphragm discharge,[157] (j) spark discharges between metal chunks,[158] (k) funnel-type reactor,[159] (l) capillary discharge.[160]

Discharges created within liquids are often close to the equilibrium,[161] which takes only a few nanoseconds to reach. Orders of magnitude of key parameters of this kind of discharges are:

- Electron density $n_e = 10^{18}$-10^{19} cm^{-3};
- Initial pressure P_0 = ~100-1000 bars;
- Initial temperatures $T_r \sim T_v \sim T_e < 1$ eV;
- Current I ~ 1-10 A.

III. A SIMPLIFIED SKETCH OF EVENTS

The fastest voltage rise time used to generate discharges in liquids is around 150 picoseconds.[162] For the synthesis of nanoparticles, it is always beyond 2 nanoseconds (*i.e.* within the so-called *short* time scale) and can extend to the second time scale. This means that typical phenomena found in target ablation by femtosecond and even picosecond lasers (leading to the so-called *ultra-short* interactions) are beyond the scope of this work.

The synthesis of nanoparticles by electrode erosion using discharges in liquids can be described by the following simplified chronological sketch of events (**Fig. 3**).[163]

Before plasma ignition, charges are injected into the liquid during the pre-breakdown phase. Either electrons are injected at the cathode or impurities (and even the liquid itself if it is aprotic) can be split into ion pairs of opposite charges at the anode. Charge injection drives the electrohydrodynamic movement of the liquid, possibly leading to turbulent flows. Once charges are injected in the liquid, breakdown occurs when the liquid density becomes low enough to enable charge multiplications. When the discharge ignites, if the dissipated power is high enough, a shockwave can be emitted. The current flows back and forth across the electrode-liquid interfaces. Both electrodes are submitted to these current oscillations that can be described by a damped RLC circuit. The discharge volume extends towards the ground electrode under the electric field, forming an ionized channel that crosses the inter-electrode gap, typically in several nanoseconds for sub-millimetric gap distances, a bit like streamers in dielectric barrier discharges. When the channel reaches the ground electrode, the voltage drops suddenly, transforming the discharge channel into an arc discharge. The electrodes, on contact with the high-temperature arc discharge, start melting after a few hundred nanoseconds, releasing a metallic vapour in the discharge. Once the metallic vapour is emitted, nanoparticles are synthesized by condensation. Other erosion processes may also be involved, depending on the conditions, leading to different size distributions. Produced particles are next transferred into the liquid phase. Once the discharge phase stops, the gas volume it occupied expands and collapses several times within the millisecond time scale, leading to bubble oscillations.

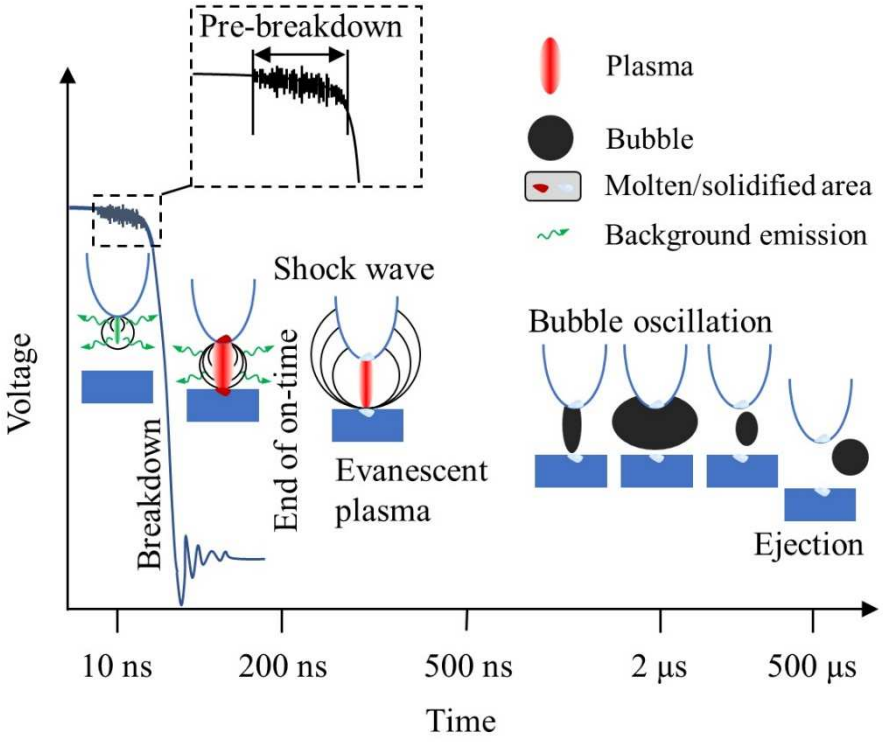

Fig. 3: Simplified sketch of events occurring in submerged discharge processes.

An energy balance is useful at this stage.[164] Basically, the largest part of the energy delivered by the source is used to create the plasma (~95%). Electrode erosion consumes only about one percent of the total energy (~1%), whereas the bubble dissipates a few percent (~5 %). The amount of energy spent in the shockwave is almost negligible (<0.1%). Of course, these figures are affected by the type of discharge used, the inter-electrode gap distance, the nature of the liquid, etc. However, we readily understand that the overall yield of nanoparticles production is a key issue in this kind of process, even though large quantities of nanoparticles can be produced because of high production rates (typically ~100 mg h^{-1} and up to 10 g h^{-1}).[89]

IV. ELECTRODE EROSION

Electrodes can be eroded by different mechanisms. This produces impacts with complex shapes. As mentioned previously, some recently identified ablation mechanisms in laser processes with ultra-short time scale (from a few femtoseconds to a few picoseconds) will not be considered.[165,166]

A. Erosion mechanisms

At short pulses, thermal processes must be considered, which is not true for ultra-short processes. The melting of the electrodes by the discharge is the most important mechanism that leads to particles synthesis. The modelling of the process is generally attuned to those developed for the description of arc–surface interaction in domains like welding or circuit-breakers. [167–169] However, several other mechanisms are possible, depending on experimental conditions. Whatever the conditions, the mean

energy of ions in these high-pressure discharges is too low to promote any sputtering effect as it is too often claimed.

1. Melting and vaporization (evaporation and sublimation)

The discharge pressure at ignition is typically beyond hundreds of bars. It is still around a few tens of bars 200–250 ns after ignition, at the end of a nanosecond-pulsed discharge.[170] This means that the energy of most particles in the ionized gas is certainly too low for sputtering. The melting of metal electrodes is not due to the Joule effect either, the resistivity of the material being too low until dissolved gases start forming bubbles, which affects the material conductivity. Following Hamdan *et al.*[163], electrodes melt essentially by irradiation from the blackbody emission of the high-temperature discharge. The maximum temperature reaches a fraction of eV (typically around 5000 K), discharges being close to local thermodynamic equilibrium. As radiation is emitted similarly on either side of the discharge channel, erosion spots are similar on either electrode. The time to melting is of the order of 100 ns for a micrometric erosion spot on an aluminium electrode.

Local melting of the electrode leads to the formation of a liquid well. The bottom of the well is in contact with a mushy region if the electrode is an alloy and not a simple metal. The interface between the surface of the liquid well and the discharge is not clearly described for several reasons: the time evolution of the pressure is not well known, the existence of a plasma sheath is contentious as it should be extremely thin, the surface is likely to be unstable, etc.

The heated electrode emits a vapour either by evaporation from the molten electrode or by sublimation from the solid electrode, and this vapour condensates in colder parts where nanoparticles form. This mechanism together with nucleation (described hereinafter) is responsible for the synthesis of the smallest particles generated by discharge in liquids. Vaporization at the surface of the molten pool can be estimated as follows.[171] The rate of the atomic flux (m^{-2} s^{-1}) leaving the surface during normal evaporation and due to a pressure gradient is given by the Knudsen-Langmuir equation:

$$\dot{m}_p = \alpha \sqrt{\frac{M}{2\pi RT}} \left(P_s^{\infty} - P \right), \tag{1}$$

M is the molar mass of the evaporating molecule or atom. The factor α (<1 and depends on temperature) is called the efficiency coefficient. R is the ideal gas constant. P is the vapour phase pressure and P_s^{∞} the saturation pressure at the temperature T of the liquid surface. These quantities are related by the Rankine form of the Clausius-Clapeyron equation, assuming the latent heat of vaporization L_v constant:

$$P_s^{\infty} = P_0 \exp\left(-\frac{L_v}{R} \left(\frac{1}{T} - \frac{1}{T_b} \right) \right), \tag{2}$$

P_0 is the ambient pressure and T_b is the equilibrium boiling temperature at the ambient pressure (the normal boiling temperature). L_v is either the heat of sublimation or the heat of evaporation. If L_v cannot be considered as constant, other expressions (like Dupré or Riedel's formulas) are required.

Vaporization can also occur because of a concentration gradient.[172] The diffusive vaporization rate $\dot{m}_d$ is expressed in terms of a phase change at the surface and the subsequent transport of the vaporized species to the bulk gas phase through the mass transfer boundary layer surrounding the pool. The vaporization rate is then defined as:

$$\dot{m}_d = K\frac{MP_s^{\infty}}{RT_b}, \tag{3}$$

where K is the mass transfer coefficient given by similarity laws.

2. Spallation

What is referred to as "spallation" corresponds to material ejection driven by relaxation of the stress induced by the treatment.[98,173] Basically, the spallation of a liquid phase in contact with its mother solid phase is due to a drift in the phase diagram where the following thermodynamic pathway crosses the liquid branch of a binodal domain and enters a metastable region. This leads to the nucleation, growth, and coalescence of voids. This induces the formation of a transient foamy structure of interconnected liquid regions, and eventual separation (or spallation) of a thin liquid layer from the bulk of the target. Material spallation occurs at the liquid–solid boundary, where the spall strength is lower than that in the solid phase. However, the tensile wave is strong enough to cause the cut-off in the liquid phase, according to the applied criteria of nucleation (**Fig. 4a**).

In a liquid – the situation under vacuum being different –, the particles produced by this mechanism exhibit distribution sizes that are around 10 nm.[165] The foamy structure coarsens with time and eventually decomposes into individual droplets on the time scale of nanoseconds. The top liquid layer loses stability because of Rayleigh-Taylor instability and decomposes into large droplets, estimated to have diameters from hundreds of nanometers to tens of micrometers.[174]

3. Phase explosion, also called explosive boiling

What is referred to as "phase explosion" or "explosive boiling" is a process where a superheated surface region, expanding rapidly, undergoes a fast decomposition into a mixture of vapour and liquid droplets (**Fig. 4b**). Thermodynamically, it means that solid matter is rapidly superheated up to the thermodynamic critical temperature, at which the spinodal decomposition in vapour and liquid phase in the irradiated material occurs by homogeneous nucleation.

This is typically what can be observed when a very clean glass of water (*i.e.* without surface defects to promote nucleation of steam bubbles) is heated in a microwave oven without boiling. The superheated

metastable liquid can undergo an explosive liquid-vapor phase transition when a massive homogeneous nucleation of vapor bubbles starts, by simply touching the surface of the liquid, for instance. This phenomenon appears at much higher energy than spallation and occurs within the nanosecond time scale.[175] As for spallation, on the time scale of nanoseconds, vapor, small nanoparticles (~10 nm), and large liquid droplets are produced.

4. Droplet emission due to surface temperature gradients

Non-homogeneous distribution of surface temperature is caused by radial temperature gradients in the discharge. It can also be amplified if the discharge channel is not oriented perpendicularly to the liquid well. Because of this non-homogeneous distribution, two driving forces responsible for expulsion of the molten liquid are generated: one emanating from the recoil pressure effect caused by evaporation, and the other one from the Marangoni effect. Large (beyond 100 nm in diameters and up to hundreds of µm) droplets are produced by both mechanisms (sometimes called hydrodynamic splashing[176]) and emitted radially (**Fig. 4c**).

Recoil pressure gradient

Expulsion of large liquid droplets can be driven at sufficiently high power by the vapour recoil. This phenomenon induces a pressure that splashes the melt and residual recoil pressure redistributes the metallic melt.[100] The melt expulsion by the recoil pressure is caused by the spatial variation of the normal stress exerted by vapour pressure within the hot spot. The gradient of vapour pressure makes the melt flow outwards, from the high-pressure spot centre to the low-pressure periphery.[177]

Marangoni's effect

The Marangoni or thermocapillary effect creates a strong tangential stress on a surface submitted to large gradients. The liquid movement within the molten pool is affected by this boundary condition that is due to the dependence of the surface tension on temperature. The surface tension of liquid pure metals decreases with increasing temperature[178] and then, Marangoni's force acts in the opposite direction of the surface temperature gradient. As the temperature usually peaks at the centre of the well, the liquid flows from the centre to the spot edge, which contributes to the expulsion of the melt. At high heating rates and small thicknesses of the molten layer, Marangoni's stresses can lead to the rupture of the molten layer,[179] melt spattering, and formation of droplets.[180]

5. Bursting bubbles

The emission of droplets from the molten well is possible via bursting of bubbles formed in the liquid. Bubbles within the molten well can be created from boiling of the liquid metal or from absorption of discharge gases.[181] Blisters are thus formed on the surface of the well.[182] A liquid film, covering the surface of the bubble, bursts and releases very fine droplets.[183] The subsequent collapse of the bubble

forms a rising jet of liquid that pinches, according to the Rayleigh-Plateau instability, and produces a spray of micron-scale droplets within tens of microseconds. (**Fig. 4d**). The effect of the electric field on the ejection of droplets from bubbles bursting at the liquid surface was considered by Holgate and Coppins.[184]

B. Shapes of eroded areas

The different shapes of eroded areas, produced by the mechanisms described previously, are depicted in **Fig. 4**. Of course, these mechanisms can combine over sufficiently large time scales, and give more complex structures. However, most of the eroded areas exhibit these shapes that are the most commonly encountered. Roughly, the size of a crater is a linear function of the square root of the electrical charge dissipated during the discharge process.[185]

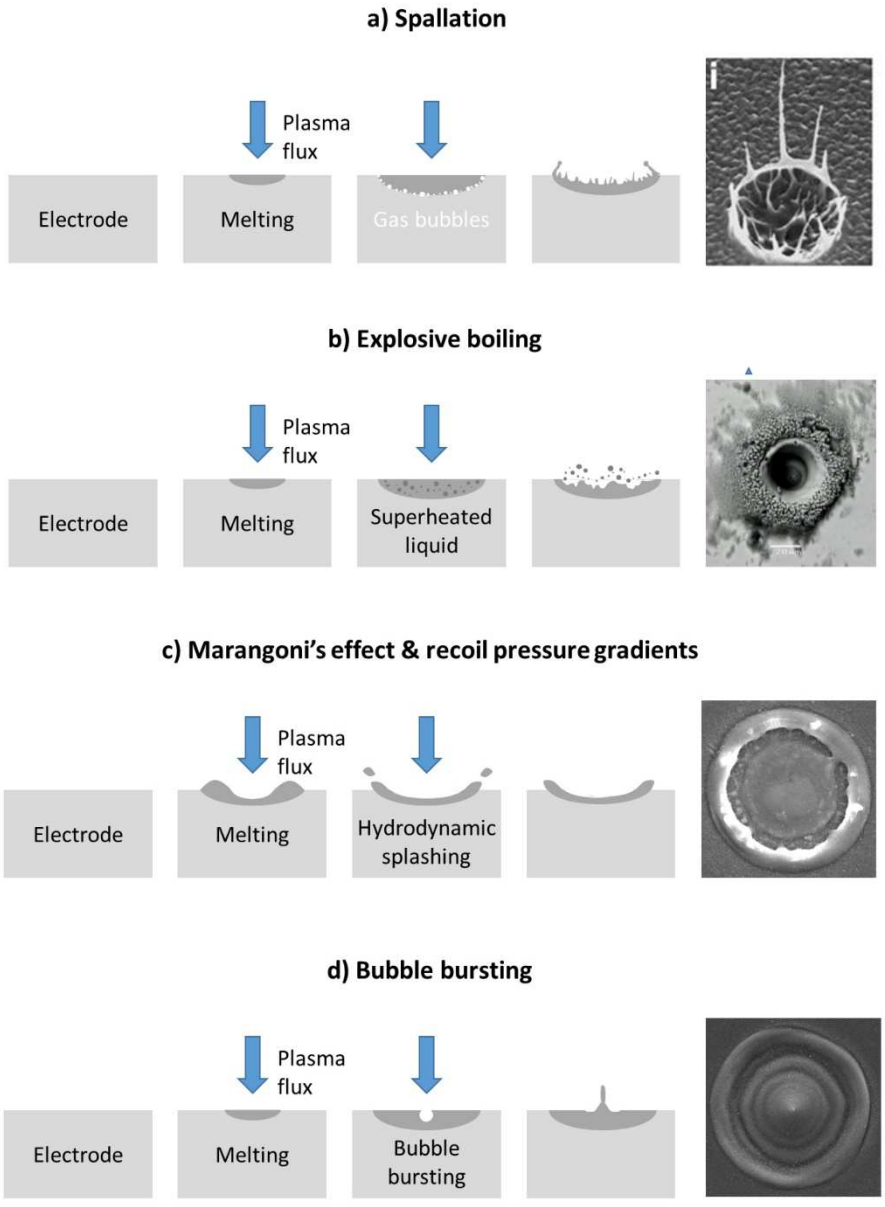

Fig. 4: Typical shapes of impacts and related underlying mechanisms leading to the production of large particles. Pictures in a) and b) are reproduced with permission from Phys. Procedia 86, 66 (2017). Copyright 2017 Elsevier. (Fig. 1 in Ref. 186) and from Mater. Res. Bull. 48, 3268 (2013). Copyright 2013 Elsevier. (Fig. 4 in Ref. 187). Other pictures are current authors'credits. All spot sizes are around 10-20 µm in diameter.

C. Limited erosion

It is possible to strongly limit electrode erosion by using materials with high melting points (usually tungsten) and low current density.[134,135] When nanoparticles are synthesized from a liquid precursor, this point is critical to keep the as-produced nanofluid with high purity.

V. THERMODYNAMICS

When the size of a particle shrinks, its thermodynamic properties changes. The Gibbs free energy of nanoparticles, made of one element, is determined by the bulk free energy and the surface free energy for both the solid and liquid phase.[188] Surface atoms are dominant for the size effect on the thermodynamic properties of nanoparticles. On the basis of the Gibbs free energy, thermodynamic properties of nanoparticles, such as melting temperature, molar heat of fusion, molar entropy of fusion, and temperature dependences of entropy and specific heat capacity can be determined.

Thermodynamics of alloy nanoparticles is still under debate, as recent results showed the existence of multiple local energy minima submitted to local thermal fluctuations.[189] The way phases separate during ultrafast cooling is difficult to predict. In simple systems like, for instance, two-element alloys undergoing eutectic decomposition with a wide miscibility gap, several situations can be encountered:

- The boundaries of phase compositions as well as transition temperatures are changed. It is the case of the Sn-In system (**Fig. 5a**).[190]
- The decomposition mechanism changes. In the Cu-Ag system, phase separation at the nanoscale occurs above 5 nm particle diameters in the 15 and 30 at.% Ag composition range.[191] The separation into Cu-rich and Ag-rich domains takes place by spinodal decomposition. Phase separation no longer occurs at nucleation sites but through the whole particle at once (**Fig. 5b**).
- The decomposition follows a specific path that leads to metastable phases that cannot be described by the two previous approaches. For instance, supercooled Au-Si nanoparticles exhibit a unique metastable phase δ_1 which grows heteroepitaxially to Au.[192]

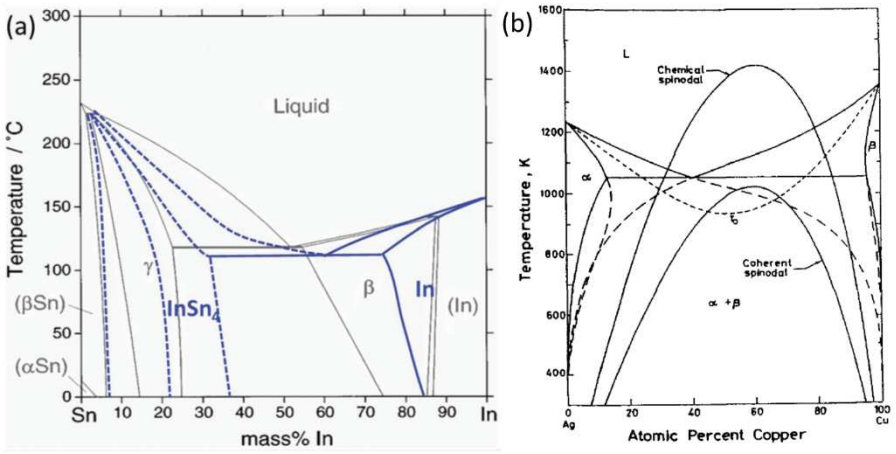

Fig. 5: Examples of metastable phase diagrams. a) Full range metastable phase diagram of Sn/In nanoparticles comparing with the equilibrium phase diagram. Reproduced with permission from Acta Mater. 123, 82 (2017). Copyright 2017 Elsevier. (Fig. 11 in Ref. 191). b) Calculated chemical and coherent spinodal boundaries in the Ag-Cu system. Reproduced with permission from Script. Metall. Mater. 29, 1131 (1993). Copyright 1993 Elsevier. (Fig. 1 in Ref. 193)

Then, resorting to metastable phase diagrams is a first approach, which cannot be considered as highly predictable. As an illustration, there are more than 20 metastable Au-Si crystalline phases that have been identified to date.

Eutectic and spinodal decompositions are not easy to distinguish in nanostructures. The Cahn-Hilliard approach predicts the critical wavelength λ_c over which fluctuations of compositions occurs in spinodal decomposition. This approach is based on the following equation:

$$\frac{\partial \rho_i}{\partial t} = \tilde{D}_{ij} \frac{\partial^2 \rho_i}{\partial x^2} - \frac{2\tilde{D}_{ij}}{f_0^{''}} \kappa \frac{\partial^4 \rho_i}{\partial x^4}, \tag{4}$$

where ρ_i is the volume density of atoms i in a binary mixture made of atoms i and j, $\tilde{D}_{ij}$ is the interdiffusion coefficient, x is the spatial coordinate, t is the time, $f_0^{''}$ is the second derivative by composition of the Helmholz free energy of a unit volume of homogeneous material (See **Fig. 6a**).

κ is the gradient energy coefficient. When the system is phase-separated into high and low composition regions, $\kappa = \xi^2 kT$. ξ is a length that scales with the interface width. It depends on the crystal lattice. For an fcc structure, $\xi = a\sqrt{2T_c/(T_c - T)}$:

$$\kappa = 2ka^2 \left(\frac{1}{T} - \frac{1}{T_c} \right)^{-1}. \tag{5}$$

T_c is the maximum temperature of the miscibility gap. a is the lattice parameter. It is possible to show that the following solution:

$$\rho_i(t) - \bar{\rho} = A(t)\sin\left(\frac{2\pi}{\lambda}x\right) \tag{6}$$

satisfies Eq.(4), which leads by substitution to the so-called amplification factor *R*:

$$R = \frac{d\ln A(t)}{dt} = -\tilde{D}_{ij}\left(1 + \frac{2\kappa h^2}{f_0^{''}}\right)h^2, \tag{7}$$

Here, $h = \frac{2\pi}{\lambda}$ and *A* is the amplitude of concentration fluctuations with a wavelength of λ. $\bar{\rho}$ is the average composition. The sign of *R* is given by the evolution of the amplitude of a concentration fluctuation with a given wavelength: if it increases, then R > 0. The critical wavelength λ_c corresponds to the condition *R* = 0. It reads:

$$\lambda_c = \sqrt{-\frac{8\kappa\pi^2}{f_0^{''}}}. \tag{8}$$

In **Fig. 6b**, λ_c is plotted versus composition.[191] The width of the miscibility gap is about 93% and the minimum of λ_c is about 6 nm at 30 at.% of Ag. With increasing Ag content, λ_c increases more and more rapidly and tends to infinity close to the spinodal composition ($f_0^{''} = 0$).

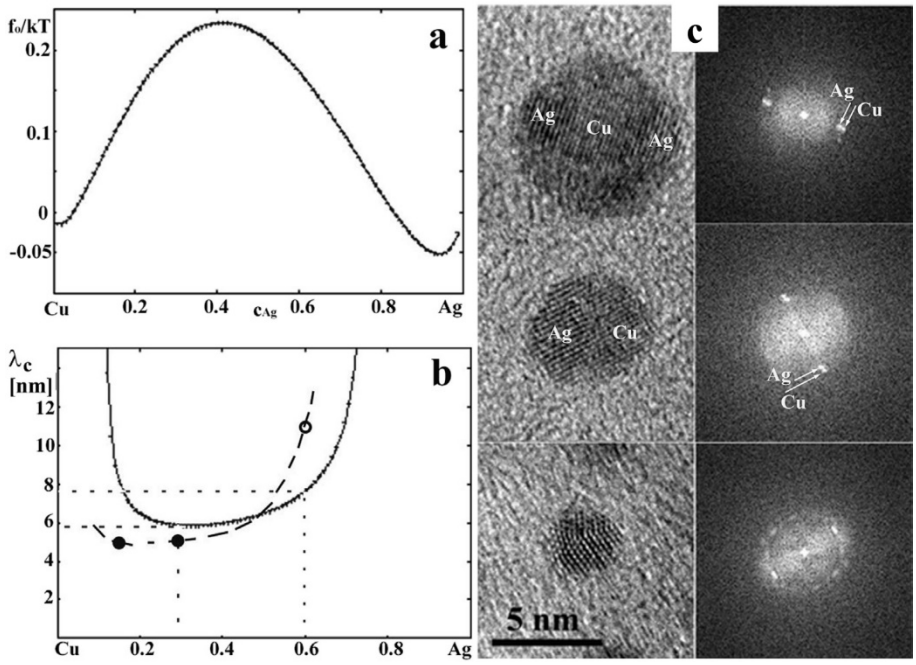

Fig. 6: (a) Homogeneous part of the Gibbs free energy f_0 and (b) critical wavelength λ_c in spinodal decomposition versus composition in Cu-Ag system (*T* = 873 K, T_c = 1053 K, *a* = 0.4 nm). In (b) full dots mark experimental critical size, the open circle marks the estimated lower value of the critical size. (c) HRTEM images of Cu-Ag nanoparticles in 30 at.% Ag particles and corresponding FFT diffraction patterns. Areas rich in silver or copper are denoted by Ag or Cu. As they contain also Cu or Ag, the

particle must not be confused with a bimetallic structure. Reproduced with permission from Acta Mater. 123, 82 (2017). Copyright 2017 Elsevier. (Fig. 3a and Fig. 8 in Ref. 191).

Consequently, we deduce from **Fig. 6b** that, below 5 nm typically, the nanoparticle cannot adopt the modulated structure of spinodal decomposition. This is observed experimentally: particles smaller than 5 nm in diameter grow as a solid solution whatever the composition (**Fig. 6c**). This shows that spinodal decomposition is both size and composition dependent. It also demonstrates that non-equilibrium alloys exist at sufficiently small scale.

VI. PARTICLES AGGREGATION AND STABILITY OF DISPERSIONS

Proper conditions are sometimes encountered for particles to aggregate, which depends on physicochemical processes at stake. Then, particles may settle, as they get bigger, on the bottom of the vessel in which they are contained. Because water is often used as primary solvent, the specific case of oxidative processes in liquid has to be specifically emphasized. Indeed, the stability of solutions is a key point in the synthesis of nanofluids. It is usually estimated by resorting to the zeta potential that derives of the electric double layer that forms around particles.

A. Aggregation of nanoparticles

Aggregation of nanoparticles, which leads to the formation of highly porous structures, is of primary importance as it generates multi-modal distributions that can compromise the application of synthesis processes of nanoparticles.[194] Irreversible aggregation of nanoparticles is well understood. The fractal formation in colloidal aggregation and the general underlying mechanism have been extensively investigated. They are well known and they can be appropriately applied on the nanoscale. Conversely, reversible aggregation still deserves to be deepened and it is only touched upon in this paper.

1. Irreversible network formation

Irreversible aggregation will be described briefly since many reference works provide comprehensive pictures of this phenomenon.[195–198]

The formation of colloidal structure and the irreversible nanoparticle aggregation are well described by the diffusion-limited cluster aggregation (DLCA) model,[199,200] a more accurate version of the diffusion-limited aggregation (DLA) model.[201] The latter considers the existence of a primary particle acting as a seed for the formation of a cluster, to which other individual particles diffuse and attach. The former describes how all particles bind to each other, and diffuse as clusters that can also attach together when in contact.

To account for the compactness of agglomerated structure, often estimated less dense than observed, the reaction-limited cluster aggregation (RLCA) model was proposed.[202,203] It relies on the idea that approaching particles aggregate with a probability less than one. This probability is defined by the

distribution of situations where the strength of the repulsion between the particles is inferior to the strength of the attraction force at shorter distances, which enables aggregation. The repulsion force is given by the Derjaguin–Landau–Verwey–Overbeek (DLVO) theory. [204,205] It accounts for van der Waals interactions and electrostatic forces arising between the double layers around the particles. This supplementary degree of freedom favours non-binding collisions between clusters, which increases their interpenetration, and produces denser structure once binding occurs. This approach was used for instance by Ziashahabi *et al*.[206] to study the formation mechanism of bead-chain-like ZnO nanostructures prepared via DC arc discharge in liquid.

In colloidal solutions, an appropriate change of the conditions destabilizes the nanoparticle suspension, and induces the aggregation of particles. The particles interact differently because their surface state changed in the new situation.[207] Forces exerted on a single particle are modified and the former balance is affected in such a way that aggregation is enabled. This results in chemical bonding, non-covalent bonding being conventionally restricted to self-assembly.

2. Reversible network formation

Aggregation of nanoparticles is expected to proceed reversibly, and the general macroscopic laws describing the irreversible network formation process are not directly useable on the nanoscale. Reversible network formation is a complex emerging topic, an example of which is as follows.

It is possible to account for the many-body van der Waals interactions on the nanoscale with so-called "many-body dispersion (MBD)" models.[208,209] Van der Waals forces between polarizable non-metallic nanostructures can be understood by collective interactions between wavelike charge density fluctuations. A simple summation over pairwise interactions between instantaneous particle- or fragment-like dipolar fluctuations is not as meaningful. The collective wavelike fluctuations are responsible for the emergence of nontrivial modifications of the power laws that govern non-covalent interactions.

Practically, there are several ways in which the modeling of the formation of nanoparticle networks is approached. A practical review on reversible network formation is available in Ref. 207). Nonetheless, a theoretical framework accounting for the reversibility of the clustering process is still pending.

B. Oxidation in liquids

Discharges are often created in liquids with different oxidation capabilities. Notoriously, water is more oxidizing than ethanol, and ethanol than ethylene glycol.[210] In general, alcohols, glycols, and hydrazine can all serve as reductant source. The choice of the liquid is also known to affect the shape of the nanoparticles.[86,145,211]

Discharges in liquids make these effects even more complicated to explain than other processes as liquids are transformed by discharges. Indeed, by-products resulting from liquid-discharge interactions are likely to play a role on the nucleation and growth of nanoparticles.

In the case of water, where air gases dissolve, chemistry is extremely complicated. It includes as main species H_2O, O_2, N_2, $OH•$, $H•$, $O•$, $N•$, H_2O_2, NO_x, O_3, HNO_2, HNO_3, $NO•$, ONOOH, and ions.[212] Species responsible for oxidation are likely to be several, but the way oxidation occurs is still unclear.

Simple description explaining how ethanol molecules scavenge OH radicals, and generate reducing species (H and H_2):[213,214]

$$OH + C_2H_5OH \rightarrow H_2O + C_2H_4OH \quad (a)$$

$$e_{aq}^- + C_2H_5OH \rightarrow H + C_2H_5O^- \quad (b)$$

$$H + C_2H_5OH \rightarrow H_2 + C_2H_4OH \quad (c)$$

is put forward to explain how non-oxidized metal nanoparticles can be produced by discharges in ethanol. Similar reasoning can be applied to ethylene glycol as metallic nanoparticles can be produced as well (see *e.g.* Refs.215 and 216).

More complex mechanisms are certainly at stake, as in the case of carbonaceous liquids or liquids containing carbonaceous additives like surfactants, where nanoparticles are often coated by a few layers of carbon.[86] Lee *et al.*[217] showed by dissolving WCl_6 in ethanol that they could synthesize spherical tungsten nanoparticles. By adding an anionic surfactant (SDS) at 30% and 50% (the surfactant/WCl_6 molar ratio), spherical particles are no longer agglomerated. A weak fraction of triangular and hexagonal-shaped nanoparticles are also found. The presence of carbon is not studied but is very likely. Generally, the balance between a too large quantity of surfactant, leading to carbon contamination and a too small quantity, leading to no effect, can only be determined by a trial and error procedure.

C. Stability of dispersions

Because of the importance of nanofluids in many industrial applications, it is essential to ensure a high stability of the dispersion in order to maintain the fluid properties constant in time. The physicochemistry of nanoparticles in liquids is a complex topic, and the examples of gold and silver will be taken to illustrate this aspect. Next, the concept of electrical double layer will be introduced to explain how the zeta-potential is defined, a useful quantity to evaluate the stability of dispersions.

1. Physicochemistry: examples of Ag and Au

The synthesis of gold nanoparticles by femtosecond laser ablation in aqueous solutions produces colloidal Au nanoparticles that are characterized by their surface hydroxylation.[218] Au-O compounds, followed by a proton loss to give surface $Au\text{-}O^-$, results in the negative charging of the nanoparticles.

This increase in the net surface charge of particles limits their coalescence, due to electrostatic repulsion. If n-propylamine is added to the solution, amine groups react with the nanoparticle surface. This is accompanied by the reduction of the particle size, which indicates that functionalization of Au nanoparticles is likely achieved during their formation by laser ablation.

On the contrary, for silver[219] (but also for iron[220] for instance), surface oxidation affects the stability of the dispersion. Nanoparticles synthesized in solutions can be stabilized by adding sodium dodecyl sulfate (SDS) as a surfactant. The surfactant coverage and the charge state on the nanoparticle surface are closely related to the concentration of SDS, which finally determines the stability of the nanoparticles in the solutions. The nanoparticles tend to be aggregated when the coverage is less than unity, while they are very stable when the surface is covered with a double layer of the surfactant molecules. High stability can be achieved as well by using isopropanol, in absence of additional capping agents. The liquid undergoes a self-inhibited free radical chain mechanism, generating the organic stabilizing agent that covers particles and stabilize them.[221]

The stability of the suspension can also be affected by the evolution of the solvent itself that may age or react with chemicals from the gas environment it is in contact with. Another possibility showed recently is water splitting during pulsed laser ablation of metal targets in water.[222,223]

2. Electric double layer (EDL)

The electrical double layer on the surface of a nanoparticle is based on the Gouy-Chapman-Stern model explaining how a surface charge, created by dissociative ionization of surface molecules, is counterbalanced by ions in the electrolyte. Basically, the double layer is made of the Stern (inner) layer where the ions are strongly bound and the Gouy-Chapman diffuse (outer) layer where the ions are loosely bound. Within the diffuse layer, there is a virtual boundary below which ions and particles behave as a whole. This boundary, placed at the zeta potential, is known as the surface hydrodynamic shear or slipping plane. Consequently, when a particle moves in an electrolyte, ions below the slipping plane move along, contrary to ions beyond the plane.

Because a nanoparticle is surrounded by the electrical double layer that sizes one Debye length, its movement can be affected by electric fields.[224] It turns out that the EDL can be polarized under the influence of external fields. This plays an important role in the accurate evaluation of the electrophoretic motion of particles.[225]

There are three main polarisation mechanisms: EDL, volume and field polarisations.

The EDL polarisability of charged species can be calculated by the Maxwell–Wagner theory from the permittivities and conductivities of the species and the medium. For a colloid, the concept of surface conductivity must be introduced and its polarizability is given by the Maxwell–Wagner–O'Konski theory.[226,227] EDL polarization cannot be neglected when the Debye length is comparable to the colloidal

size, the zeta potential is moderately high, and/or the applied frequency of the external electric field is of the same order as the rate of ionic diffusion over the colloidal size.

In volume polarisation (**Fig. 7**), the positive and negative ions in the liquid are migrating under the influence of the external field. As these ions cannot penetrate the colloid, the volume of the particle acts as a physical obstacle, which hinders the migration. The subsequent accumulation of charges of opposite signs on either side of the particle induces a dipole moment anti-parallel to the external electric field.

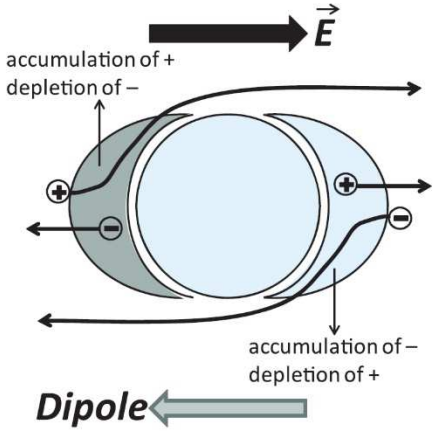

Fig. 7: Illustration of the volume polarisation effect created by an accumulation of negative ions on one side of the particle with negative surface charge, while positive ions are depleted in this region. The induced dipole moment points from the front side toward the back side will be formed and is anti-parallel to the external electric field. Reproduced with permission from Molec. Phys. 113, 2511 (2015). Copyrights Francis & Taylor. (Fig. 12 in Ref. 225).

Field polarisation is due to the Coulombic attraction/repulsion between a charged colloidal particle and the clouds of surrounding ions. Counter-ions/co-ions tend to accumulate in the tail of the particle as they circumvent the particle, resulting in a dipole moment proportional to the external electric field. This effect is observed for highly charged particles with high zeta potential, the induced dipole moment being then proportional to the external electric field.

VII. PARTICLES' LIFE

Particles' life starts by nucleation, nuclei becomes seeds, and seeds nanocrystals. What is meant by seeds is an intermediate object between a nucleus and a nanocrystal, in which no structure fluctuation (*i.e.* changes of bond-orientational order)[228] is possible. From their formation to their transfer into the liquid phase, nanoparticles are submitted to complex environments where huge gradients prevail. Even though discharges in liquids are often close to equilibrium, nanoparticles can adopt complex shapes.

A. Shape control

The shape and structure of Au or Ag nanocrystals strongly affect their spectroscopic properties (like localized surface plasmon resonance,[229] surface-enhanced Raman scattering,[230] Surface Enhanced

Fluorescence[231], plasmon enhanced optically stimulated luminescence,[232] etc.), enabling Enhanced Spectroscopies, reviewed for example in the following contributions.[233-235]

1. From atoms to nuclei

Classical nucleation theory stipulates that the formation of nuclei in supersaturated homogeneous solution is governed by the balance between the bulk and surface energy of the new phase.

$$J_{nucl} = A\exp\left(-\frac{E_a}{k_B T}\right)\exp\left(-\frac{\Delta G_{ex}}{k_B T}\right), \tag{9}$$

The first exponent ($-E_a / k_B T$) is related to the kinetic barriers with an overall activation energy E_a, while the second exponent ($-\Delta G_{ex} / k_B T$) represents the thermodynamic barrier. The parameter A is a pre-exponential factor that depends on the properties of the investigated material. It is possible to predict nucleation rates from this equation for any material at a given level of supersaturation.

However, as discussed by Gebauer *et al.*[236], values calculated accordingly can differ by orders of magnitude from experimentally measured data. Non-classical nucleation theories are then needed but are beyond the scope of this work.

2. From nuclei to seeds

The shape of a single crystal at equilibrium in an inert gas at low temperature (rigorously 0 K) or vacuum can be determined by the Wulff construction. For a fcc metal, possible shapes correspond to polyhedrons (truncated octahedrons). However, the final shape adopted by a fcc nanocrystal can differ a lot from Wulff's shapes. This deviation can be attributed to several reasons:[210]

- nucleation and/or growth are far from equilibrium,
- surface energies are modified by a capping agent, impurity, or solvent,
- twin defects affect nucleation and growth and lead to new shapes such as decahedron and icosahedron with a total free energy lower than that of Wulff's polyhedrons,
- the synthesis temperature is high.

There are three main ways to control the shape of nanoparticles.

Interfacial energy

Discharges in liquids are often near thermodynamic equilibrium. The shape of nanoparticles is then controlled by the interfacial free energy, γ. It can be defined as the energy needed for creating a unit area of new surface:

$$\gamma = \left(\frac{\partial G}{\partial S}\right)_{n,T,P} = \frac{1}{2} N_b \varepsilon \rho_s , \tag{10}$$

where G is the free energy and S the surface area. For a given surface, N_b is the number of broken bonds, ε the bond strength, and ρ_s the atom surface density. For an fcc structure with a lattice constant of a, one finds easily that:

$$\gamma_{111} = 4.24 \times \frac{\varepsilon}{a^2} < \gamma_{100} = 4 \times \frac{\varepsilon}{a^2} < \gamma_{110} = 3.36 \times \frac{\varepsilon}{a^2}, \quad (11)$$

Then, single-crystal seed takes an octahedral or tetrahedral shape in order to maximize the expression of {111} facets and minimize the total surface energy. These inequalities can be modified by the introduction of twin defects. The strain energy caused by twin defects greatly increases as the seed grows in size. This critical dependence on size is also sensitive to reaction kinetics, which offers a possibility of control.

Kinetics limitation

If the reaction that forms the atoms building the particle is slow, nuclei and seeds form through random hexagonal close packing (rhcp), together with the inclusion of stacking faults.[237] This limitation by a kinetically controlled step makes seeds adopt shapes that depart from those favoured by thermodynamics. Inclusion of stacking faults and/or twin planes can thus lead to the formation of plate-like seeds.

The key is to ensure an extremely low concentration of metal atoms, so the nuclei will not be able to grow auto-catalytically into polyhedral structures. Instead, the atoms will add to the edges of a planar cluster to generate a plate-like seed. This was observed (Refs. 130 and 202) by forming plate-like lead particles using discharges in liquid nitrogen (**Fig. 8**).

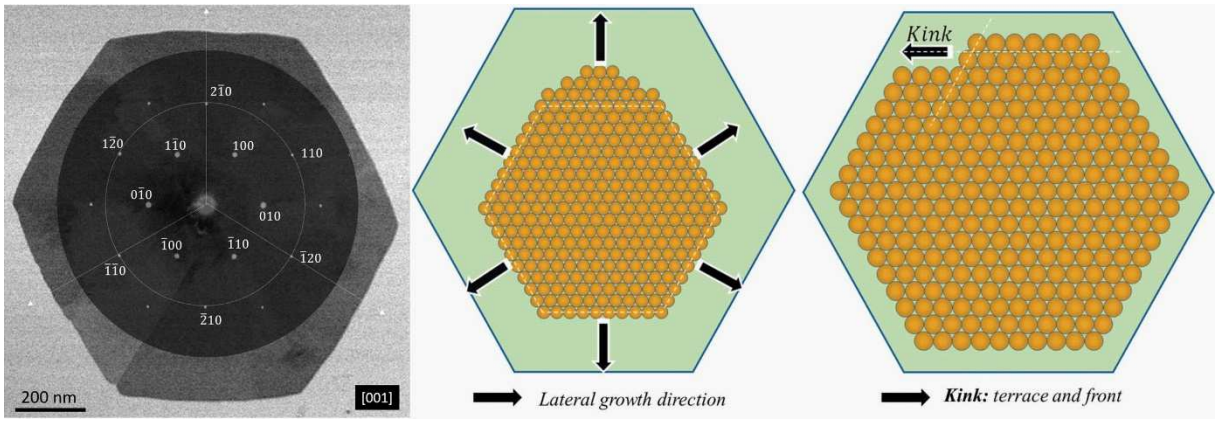

Fig. 8: Left: Diffraction pattern of a PbO_2 single crystal superimposed on the TEM bright field micrograph. Oxidation occurred after air exposure but growth corresponds to Pb in liquid nitrogen. The arrows show directions that are perpendicular to the growth of the hexagon faces. The zone axis is [001]. Reproduced with permission from Particuology 40, 152 (2018). Copyright 2018 Elsevier. (Fig. 7 in Ref. 148). Middle and right: Schematic representation of the radial growth of the lead nanosheet. Reproduced with permission from J. Appl. Cryst. 52, 304 (2019). Copyright 2019 IUCr. (Fig. 8 in Ref. 238)

Oxidative etching

Hieda *et al.*[135] produced gold nanoparticles whose shape was progressively etched and decreased in size during the treatment beyond 5 min by changing the composition of the colloidal solution (initially water containing $HAuCl_4 \cdot 4H_2O$ and sodium dodecyl sulfonate). Successive discharges create H_2O_2 species and lower the pH value, leading to new conditions where nucleation stops, and etching is enabled. This is also what Saito *et al.*[79] observed in similar experiments (**Fig. 9**).

Xia *et al.*[210] give a more accurate view of oxidative etching. The distribution of single-crystal versus twinned seeds can be further modified by oxidative etching, in which zero-valent metal atoms are oxidized back to ions. If a ligand for the metal ion is also present in the same solution, a combination of the ligand and O_2 can result in a powerful etchant for both the nuclei and seeds.

Consequently, we can readily understand how discharges in colloidal dispersions contribute to the shaping of nanoparticles. As the discharge runs, production of oxidizing species (among which H_2O_2) progressively modifies the liquid composition by reacting with ligands and by forming etching agents. However, these mechanisms have not been clarified yet in the case of discharges in liquids.

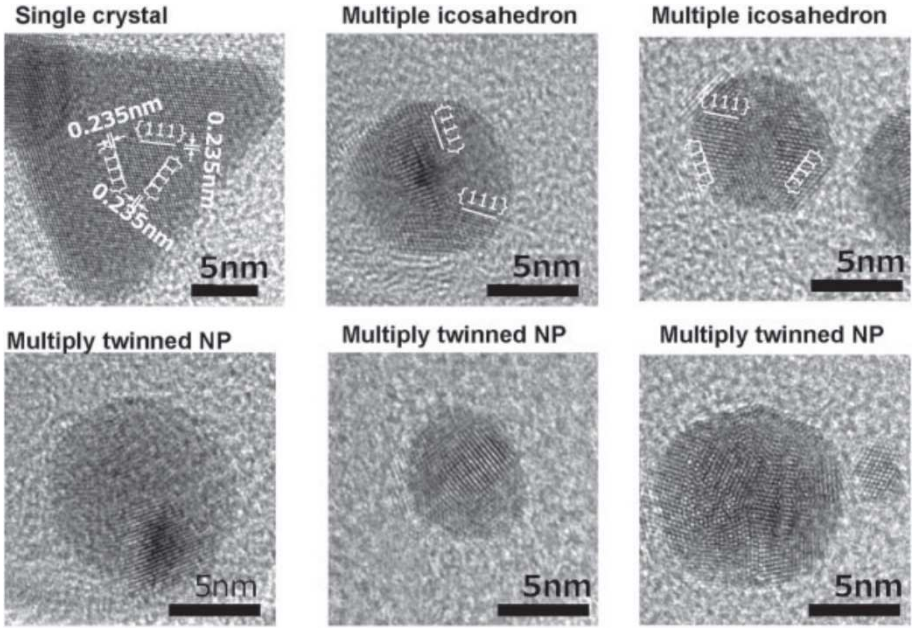

Fig. 9: HRTEM images of gold nanoparticles synthesized by discharges in reverse micelle solution. The synthesized gold nanoparticles have different crystal features like fcc single-crystalline particles, multiply twinned particles, and incomplete multiply twinned particles (single-nanotwinned fcc configuration). Reproduced with permission from Jap. J. Appl. Phys. 57, 0102A4 (2018). Copyright 2018 The Japan Society of Applied Physics - IOP Science. (Fig. 7 in Ref. 79).

3. From seeds to nanocrystals

The condensation mechanism for the growth of nuclei, *i.e.*, deposition of atoms or molecules on the surface of growing particles, the condensation rate can be approximated by the collision rate of monomers with the nucleus:[239]

$$v_{cond} = v_{th}\rho(r_0 + r_n)^2, \tag{12}$$

The average thermal velocity of the monomers in the gas is given by $v_{th} = (8k_BT/\pi M)^{1/2}$, where ρ is the monomer density, r_0 and r_n are the hard sphere equivalent radii of a monomer and a cluster. In this expression for the condensation rate, the cross section is taken as the surface area of a sphere of radius r_n and the sticking probability upon collision is equal to 1.

Consequently, if this probability is not 1 but dependent on facet orientation, the shape of a crystal can change if there is a mix of different facets on the surface. For example, when metal atoms add to the {100} faces of a nanocube, they migrate to the edges of the face resulting in the elongation of the {111} facets. Progressively, the cube transforms into a cuboctahedron and eventually an octahedron. This shape evolution process is known as overgrowth.

The introduction of a capping agent can alter the growth rates of the different facets, thus dramatically altering the final nanocrystal shape. In discharges in liquids, sodium citrate,[131,138] reverse micelle solution (sodium bis (2-ethylhexyl) sulfosuccinate in dodecane),[240] sodium dodecyl sulfonate,[135] cetyltrimethylammonium bromide (CTAB),[241] among many other capping agents, are used, from recipes developed for chemical processes.

It is important to mention that surfactants and capping agents are very difficult to decompose completely, which results in poor catalytic activities. Discharges in liquids are often presented as efficient methods to synthesize nanoparticles without any surfactant.

B. Other phenomena affecting size

Nanoparticles within the discharge can melt, be vaporized or coalesce, leading to changes in size distributions.

1. Melting

The melting point of a spherically symmetric nanoparticle decreases as the radius decreases, which is only observed at very low radius (typically below 10 nm).[242] This effect can be described down to about 1 nm for gold[242] or nickel[243] by using a continuum model (**Fig. 10**). Melting point depression is often accounted for by the generalized Gibbs–Thomson implicit relation:

$$L_m\left(\frac{T_m}{T_m^*}-1\right)+\Delta c_p\left[T_m\ln\left(\frac{T_m}{T_m^*}\right)+T_m^*-T_m\right]+2\frac{\sigma_{sl}}{\rho_s}\kappa=\left(\frac{1}{\rho_l}-\frac{1}{\rho_s}\right)(p_l-p_a), \tag{13}$$

L_m is the latent heat [J kg^{-1}], T_m the temperature at which the phase change occurs [K], T_m^* the bulk phase change temperature [K], c_p is the specific heat [J kg^{-1} K^{-1}], $\Delta c_p = c_l - c_s$, σ the surface tension [N m^{-1}] and κ the mean curvature. ρ is the density [kg m^{-3}]. p is the pressure [Pa]. Subscripts a, s and l indicate ambient, solid and liquid, respectively.

Surface atoms are less strongly bound to the cluster than bulk atom. Then, melting proceeds by separation of surface atoms from the bulk. This separation is paid for with the latent heat. With a sufficiently large cluster, the energy required is relatively constant since each surface molecule is affected by the same quantity of bulk molecules. However, as the cluster decreases in size, surface molecules are less and less influenced by the bulk, and less and less energy is required for separation. The change in the ratio of surface to bulk energy may also lead to a structural transition and a reduction in surface tension.

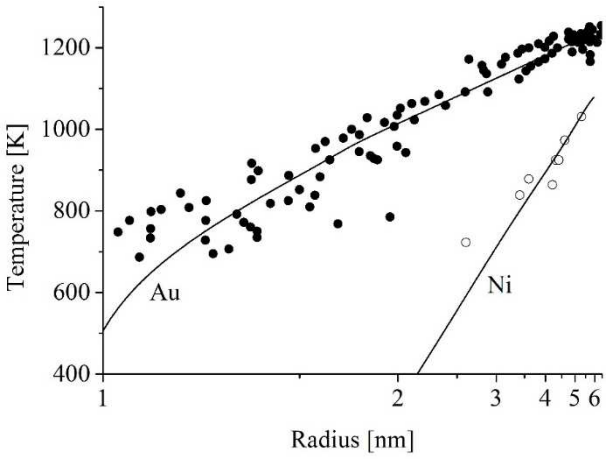

Fig. 10: Experimental data and Gibbs-Thomson curves established from Eq. (1) showing the size dependence of the melting temperature of gold[242] and nickel[243] nanoparticles in an (Y – 1/X) graph. The behaviour is almost linear beyond 2 nm in this graph and follows a reciprocal law.

2. Vaporization

Once the vapour is emitted from the electrode, it condensates farther in colder regions into droplets that are still prone to vaporization along their path. Vaporization of a nanodroplet is affected by the particle size. The equilibrium pressure at the surface of the droplet (**Eq. 2**) must be corrected.[244,245] The correction is:

$$P_s^r = P_s^\infty \exp\left(\frac{2\sigma M}{\rho RT} \times \frac{1}{r}\right), \tag{14}$$

P_s^r is the saturation pressure for a droplet of radius r. σ the surface energy and ρ the density.

3. Coalescence

Coalescence affects the size distribution of nanoparticles by merging primary particles, *i.e.* those produced by condensation, into a larger single nanoparticle (see **Fig. 11**). This is a very complex phenomenon between nanocrystals that can be decomposed into elementary steps:[246]

1) *Coagulation* refers to the attraction and contact between primary particles. In the discharge, it is due to in-flight collisions after which particles remains stuck together. This phenomenon is often referred to as Smoluchowski ripening.[247]

2) *Rigid body reorientation* occurs once the primary particles are close enough to start interacting. An interface forms that is usually misoriented, because of the randomness in the coagulation geometry. Thus, a number of interface layers are shorn. Eventually, the particles rotate as rigid bodies, driven by mutual torques, maximizing the contact area. A more coherent interface with a larger area is then produced.

3) *Formation of defects* results from the very fast (few ps) reorientation stage. If primary particles cannot be perfectly aligned because of their geometry, which is the most probable situation, a twin boundary – commonly accompanied by the appearance of misfit dislocations – forms, as rotation is hindered by the newly formed bonds.

4) *Heat release* results from free-surface annihilation due to bond formation. As the surface/volume ratio decreases, the part of the surface energy remaining after the creation of the interface transforms into thermal energy.[248]

5) *Temporary melting of interface* has been proposed by Grammatikopoulos *et al*.[249] If the heat release essentially contributes to the temperature rise of the child particle (case of an adiabatic system), it can be sufficient to reorganize it at the atomic level. A wave that originates at the interface between the primary particles, propagates along the body of the child particle, resulting in its full crystallization. Concurrently, a temporary disordering of the atoms at the interface and a "softening" of their bonds is observed.

6) *Neck growth* is all the more fast as local curvature is high, which speeds up atomic surface diffusion. A neck is formed on either side of the interface when primary particles coagulate. However, the neck only reaches substantial dimensions if it is promoted by the temporary melting of the interface that enhances the transport of atoms from the core of primary particles to the neck.

7) *Plastic deformation*. Even after neck formation, the system can still behave within the elastic limit (~0.8 nm after Averback and Zhu[250]) as a coupled-oscillator (with possible rotation of the two primary particles). Thermal vibration makes each particle pulsate around the initial contact locus. Plastic deformation is then possible by relaxation of accumulated internal shear stress, possibly assisted by the heat, which enables the glide of misfit dislocations and their annihilation at the surface. Protrusions can thus be formed.

8) *Consolidation*. The neck thickens at a growth rate that slows down, because the difference in curvature between the neck and the primary particles becomes smaller. The two-particle system gets stiffer, which hinders its pulsation, and makes it behave as a single particle. Consolidation takes about 100–200 ps. Free-surface annihilation becomes negligible, and so the heating it induces. Oftentimes, experimentally grown nanoparticles are trapped in a metastable steady state due to quenching upon deposition. Coalescence is often considered as achieved at this point in theoretical approaches.

9) *Slow ageing*, however, extends the coalescence process and favours a "sphericization" of the system, as referred to by Lewis *et al.*[251], a process that lasts for hundreds of ns up to a few µs. This means that the ratio of the surface area of the particle tends toward the surface area of a sphere of the same volume as the particle. Here, the neck acts as a sink for diffusing atoms.

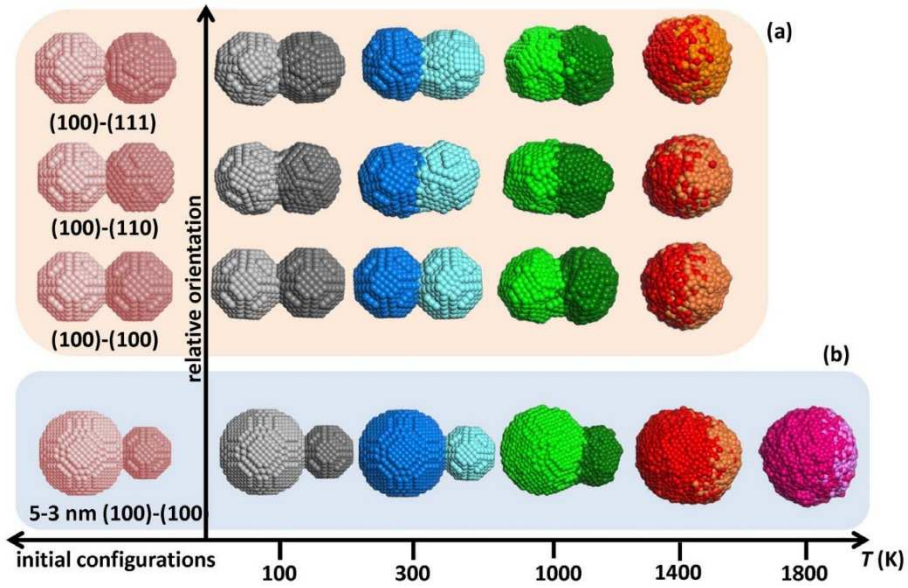

Fig. 11: Parameters affecting nanoparticle coalescence. (a) Effect of temperature and relative orientation on the coalescence of 2 crystalline Pd nanoparticles, 3 nm in diameter. (b) Effect of temperature and size on the coalescence of 2 crystalline Pd nanoparticles of different sizes (5 and 3 nm in diameter), with touching (100)-type facets. Note that (b) is not to scale with (a). (For clarity, temperatures are represented by shades of colours). P. Grammatikopoulos, C. Cassidy, V. Singh and M. Sowwan, Sci. Rep. 4, 5779 (2014); licensed under a Creative Commons Attribution (CC BY) license. (Fig. 2 in Ref. 249).

4. Oxidation in air

Except for gold, nanoparticles produced by submerged discharges are prone to be oxidized either in air, when they are floating on or taken out of a non-oxidizing liquid. They can also be oxidized on purpose but this aspect is deemed to be beyond the scope of this article. Oxidation of sub-micrometric objects has been studied thoroughly.[252] Only oxidation in dry air at room temperature is described here. This

process changes the size of the pristine nanoparticles because of the change of molar volume between the metal and its oxides.

Basically, when the particle is less than 1 µm in diameter, electrical neutrality, assumed in Wagner's theory for thick films,[253] within the oxide layer is not satisfied, and when less than 20 nm, the Nernst-Einstein relationship is no longer appropriate. Thus, theories of thin film growth must consider atom jumps in the presence of large electric fields and the possibility of large space charges.

Cabrera and Mott's theory assumes that electrons can freely pass from the metal to ionize adsorbed oxygen atoms or molecules at the oxide/gas interface, so that the electron electrochemical potential (Fermi level) is equal in the metal and the adsorbed gas layer.[254] The general picture is based on the injection of defects into the oxide at one of the film interfaces (with gas or metal). This process is assumed to be rate-controlling. Using the Kröger-Vink notation, and taking the example of chromium oxidation, one notices that, depending on the temperature and O_2 partial pressure, either triply charged chromium vacancies are injected at the gas/oxide interface and diffuse inward:

$$\frac{3}{2}O_2 \rightarrow 3O_O^x + 2V_{Cr}^{'''} + 6h^{\bullet} \qquad \text{(p-type } Cr_{2-x}O_3\text{) – gas/oxide interface}$$

or triply charged interstitial chromium atoms are created at the metal/oxide interface and diffuse outward:

$$Cr_2O_3 \rightarrow 2Cr_i^{\bullet\bullet\bullet} + 6e^{'} + \frac{3}{2}O_2 \qquad \text{(n-type } Cr_2O_{3-x}\text{) – metal/oxide interface}$$

In both cases, the accumulation of vacancies at the metal/oxide interface induces the development of Kirkendall porosity. Such a porosity is not observed if the oxide growth is driven by two other types of mechanisms, observed with other metals: oxygen atoms, injected at the gas/oxide interface, diffuse inward (p-type MO_{1+x}) and oxygen vacancies, injected at the metal/oxide interface, diffuse outward (n-type $M_{1+x}O$). This explains why oxidation of some nanoparticles leads to core-shell structures and/or hollow particles.

For very thin (*i.e.* where tunnelling can no longer be neglected) films, Fromhold showed that the assumption of electronic equilibrium is reasonable.[255] In the case of nanoparticles, quantum confinement effects should also intervenes, but to best of our knowledge, no study has been done on this topic yet.

Finally, it is also important to mention that reduction of nanoparticles after oxidation does not lead to a complete recovery of the initial metallic state. For instance, after oxidation in O_2, ZnCu clusters (< 10 nm) transform into a polycrystalline cluster consisting of separate CuO and ZnO nanocrystals. Subsequent reduction in H_2 converts CuO into Cu with ZnO nanocrystal covering its surface. Then, H_2 dissociates onto metallic Cu to form H atoms that partially reduce ZnO into CuZn.[256]

These theories are based on point defects but oxidation is also affected by the presence of structural defects that play a tremendous role at low temperature, as volume diffusion is strongly limited because of high-energy barriers of jump processes. These barriers can be lowered by stress to a certain extent, which is also an important effect to take into account in order to predict correctly how oxidation occurs in these specific conditions. Finally, in air, not only oxygen but also water can intervene as oxidation agents. The reader is referred to a number of seminal papers illustrating these phenomena in the case of different elements: *e.g.* oxidation at room temperature of reduced iron oxide nanoparticles by Wang *et al.*[257], air oxidation of monodisperse cobalt nanoparticles by Varon *et al.*[258], the first stage of air oxidation by Chen *et al.*[259] or the evolution of the oxide thickness and oxidation rate of Si nanoparticles in air and at room temperature by Yang *et al.*[260]

The effect of the spherical geometry on metal oxidation driven by mobile charged point defect was also studied by Fromhold.[261] The electric potential developed across the oxide is the same as for planar geometry, but the time, for complete oxidation for spherical particles of a given diameter, can be as much as a factor of 3 shorter than that for planar samples of the same thickness.

C. More complex structures

Discharges in liquids can be used to synthesize nanoparticles made of, at least, two different materials that can be organized in different structures depicted in **Fig. 12**. Both materials are made immiscible, either because thermodynamics imposes it (**Fig. 12a to e**), or because they are synthesized successively (**Figs. 12a, b or c**).

Bi-particles (**Fig. 12a**) have been synthesized by different groups: *e.g.* Pt-Pd,[262] Ni-Cu,[241] Ag-Pt,[263] Ag-Cu,[264] etc. This kind of structures results from coalescence of particles that are synthesized either simultaneously (from electrodes made of different materials) or separately (in space and/or time). Tsukanov *et al.*[265] showed by molecular dynamics that immiscible nanoparticles can interpenetrate if they collide with sufficiently high relative velocities.

Core-shell structures (**Fig. 12b**) are usually obtained by chained treatments where seed nanoparticles of one material are coated by another material in a second step. The best way to coat nanoparticles already present in a liquid is to decompose a precursor that deposits onto the nanoparticles surface. This is easy to achieve by discharges in contact with liquids for instance.

Conversely, discharges in liquids rather form attached nanoparticles in sequenced treatment. The expansion of the discharge repels nanoparticles added in the liquid from emitted species by the electrodes. Then, one-step synthesis is only possible by mixing intimately the two elements in a crucible: *e.g.* CuO@Ta_2O_5.[123] For a carbon shell, one-step synthesis is also possible with a carbonaceous liquid, like benzene or hexane: *e.g.* (Co, Ni, Fe)@C.[266–268] Then, using a liquid precursor (like $HAuCl_4$) in a

aqueous colloidal dispersion containing nanoparticles, say Pt, should give Pt@Au nanoparticles in one step. But to the best of our knowledge, no experiment of that kind has ever been done yet.

Pulsed laser ablation also provides similar capabilities. For instance, the introduction of *ad hoc* solvents lead to the creation of carbon shell or structures.[269] Even more interestingly, the possibility of using CO_2 sub-products in solution with NaOH was showed to be efficient for the production of gold-carbon nanocomposites.[270,271]

Kabbara *et al.*[272] showed that it is also possible in two steps, by wrapping one type of particle (Cu) into an ultra-thin foil made of another one (Zn) synthesized beforehand, this mechanical way of forming core-shell nanoparticles requiring no deposition.

Decorated nanoparticles (**Fig. 12c**) are usually obtained by depositing one phase of small size onto another phase of large size. Usually, this is a two-step process. This has been achieved in one step by discharges in liquids for the Si-Sn system.[273] The mechanism relies on grain detachment of a sintered Si-Sn electrode, where Si and Sn are well separated, leading to tin nanoparticles attached to silicon grains.

Nanoparticles with multiple domains (**Fig. 12d**) are either made of one phase inlaid into another or made of one phase segregated at the grain boundaries of another. These particles, as Janus particles (**Fig. 12e**) – a special type of nanoparticles with surfaces exhibiting two or more distinct physical properties – have only been synthesized by PLAL but not by discharges in liquids.

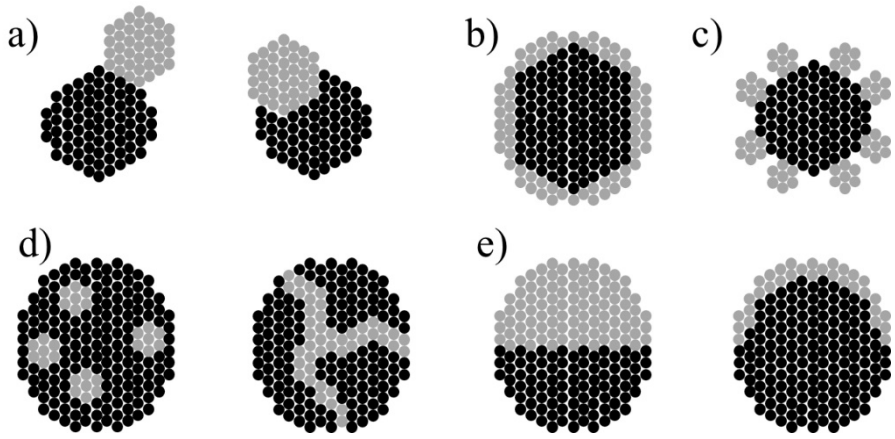

Fig. 12: Possible structures associated with bi-particles. a) bi-particles (more or less interpenetrated); b) core-shell; c) decorated; d) multiple domains; e) Janus.

VIII. PARTICLES' SIZE DISTRIBUTION

As discharges in liquids most often produce several size distributions, it is essential to describe how to measure them, which requires to master the techniques used in order to get convergent results. It is also possible to change size distributions by fragmenting nanoparticles.

A. Size distributions

Ashkarran *et al.*[130] (**Table 1**) obtained almost monodisperse (*i.e.* with a geometric standard deviation of a log-normal distribution < 1.25) gold colloidal dispersion (mean size: 8 ± 3 nm) by creating discharges between two titanium electrodes in a $HAuCl_4$ solution. This process behaves as an electrochemical process, similarly to discharges in contact with liquids. Submerged discharges in liquids where nanoparticles are produced by electrode erosion produce multimodal size distributions (**Fig. 13**).[145,274,275]

At most, three distributions coexist. Large particles (*i.e.* > 100 nm and up to tens of µm) are only a few and spread all over the substrate. Nanoparticles of intermediate size (*i.e.* from 20 to 100 nm) are found either as necklace-like or fractal agglomerated structures or as isolated particles. Nanoparticles of small size (*i.e.* from 2 to 10 nm) are primary particles.

However, this approach is not satisfactory as the various populations are not associated with their mechanisms of formation. From the list of erosion mechanisms established hereinabove, it is easy to understand that the origin of the largest population of nanoparticles is due to ejection of droplets from the liquid well but there are several possible mechanisms that may be involved. The origin of the smallest distribution can only be due to the rapid condensation of the vapour phase. On the contrary, the origin of the intermediate-size population can be multiple. The smallest nanoparticles can continue growing if they stay within the discharge region, reacting with the emitted vapour that is not homogeneously distributed within the interelectrode gap. They can also grow by coarsening with other particles and then, the distribution of the particles themselves also matters. Consequently, we could expect 4, 5 or even more contributions in a multimodal size distribution. This statement is corroborated by several works where trimodal distributions are proposed (see for instance Ref. 128 and in Ref. 150 Table 1) but with very different mode positions. The issue lies in the possibility for distinguishing accurately all the modes in a distribution of nanoparticles.

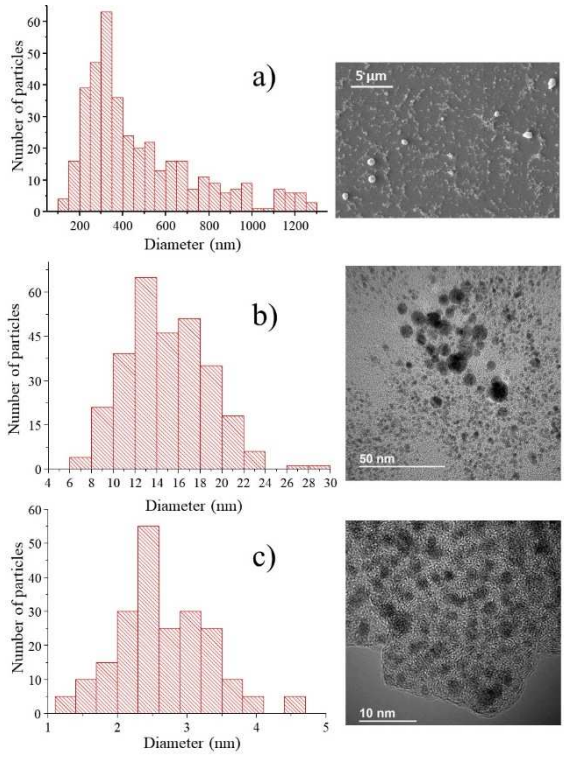

Fig. 13: Size distributions of particles produced by discharges in liquid. Three distributions are commonly found. The two lowest distributions can overlap, leading to two main distributions, as it is described in some other processes like pulsed laser ablation in liquid. Reproduced with permission from Mater. Chem. Phys. 142, 199 (2013). Copyright Elsevier. (Fig. 4 in Ref. 274).

In LASiS, nanosecond pulsed laser ablation is known to give more or less narrow monomodal distributions that are described by a log-normal distribution, ablation being principally driven by thermal processes. On the other hand, pico and femtosecond ablation may lead to multimodal distributions, due to the multiple ablation mechanisms. In this latter case, size distributions can also be sometimes by described by a log-normal distribution. Therefore, caution must be taken to interpret these size distributions.

Logically, the existence of several erosion mechanisms must lead to an identical number of distributions. However, one reads commonly that two populations are to be distinguished: small and large. In recent studies based on molecular dynamics simulation, Shih et *al.*[175,176] investigate the origin of bimodal nanoparticle size distributions produced by laser ablation in liquids. They establish that "*three distinct nanoparticle generation mechanisms operating at different stages of the ablation process and in different parts of the emerging cavitation bubble*" exist. Two of them produce large nanoparticles (spallation and explosive boiling) and one small nanoparticles (nucleation at the very front of the emerging cavitation bubble). They conclude that "*the coexistence of the three distinct mechanisms of the nanoparticle formation at the initial stage of the ablation process can be related to the broad nanoparticle size distributions commonly observed in nanosecond PLAL experiments*". To the best of

our knowledge, no attempt was made to fit with a multimodal approach, size distributions of nanoparticles produced by ns laser pulses that can be described by a monomodal log-normal function.

The confusion also exists because only the smallest nanoparticles are collected for analysis. For instance, it is possible to proceed as follows.[276] In a discharge-based process, when heavy particles settle at the bottom of the vessel that contains the synthesized colloid suspension, this latter can be cleared from its sediments by pouring carefully the upper part of the solution into another beaker. Then, small quantities of the new solution containing only its lightest particles can be collected with a pipette for further characterization.

There are several techniques that can be used to evaluate the mean diameter of a set of well-defined nanospheres: DLS (dynamic light scattering), AFM (atomic force microscopy) in tapping mode, UV-Visible spectroscopy and two-colour SPR (Surface Plasmon Resonance) spectroscopy. Several papers[277,278] showed that estimates of the mean diameter of well-controlled nanospheres synthesized by wet chemistry and evaluated by the previously-cited techniques are very close, demonstrating the convergence of these methods for almost ideal spheres. On the other hand, for other types of nano-objects, caution must be taken to interpret results produced by these different diagnostics, as discussed by Tomaszewska *et al.*[279] For example, differences between TEM and UV-Vis spectroscopy often arise due to:

- possible agglomeration of nanoparticles during deposition on the grid, especially in colloidal dispersions in water;
- non-spherical shape of nanoparticles;
- a non-representative sampling of nanoparticles for TEM analysis;
- nanoparticles are oxidized, which affects the effective dielectric constant to be used in the Mie fit required by UV-Vis spectroscopy.

The existence of an intermediate size distribution is not clearly understood yet, likely because it probably results from distinct phenomena:

- the duration of the nucleation process may strongly vary if the vapour is emitted at the very beginning of the process, when the pressure is high, or much later, when it is reduced;
- it is also true for the vapours emitted by the cathode and by the anode;
- coalescence of particles certainly affects the size distribution, and smear out transitions between modes, etc.

To conclude about size distribution, it is important to mention that even though it is a useful concept to describe the population of nanoparticles produced by a given process, it cannot be used usually to correlate observations on size modes with underlying growth mechanisms.

B. Fragmentation of nanoparticles

Until now, fragmentation of nanoparticles has not been observed with electric discharges, but this process might exist as well for sufficiently fast electric fields (picosecond-pulsed discharges). Indeed, Giammanco *et al.*[280] fragmented Au nanoparticles by interaction with the second and the third harmonics of a Nd:YAG picosecond laser. However, laser and discharge treatments are already associated in that purpose.[281]

The photothermal mechanism responsible for nanoparticle fragmentation relies on the way temperature rise in response to the laser excitation. At moderate fluences, heating, melting, and evaporation of irradiated nanoparticles enables size reduction of primary nanoparticles, creating a new population of smaller ones by nucleation and growth from the evaporated atoms. At higher fluences, nanoparticles can be either fully evaporated or fragmented by explosive decomposition into vapor and liquid droplets when superheated up to the limit of thermodynamic stability of the molten material.[282]

According to Huang and Zhigilei,[283] the detailed analysis of the nanoparticle fragmentation mechanisms reveals two distinct pathways of the formation of the fragmentation products: (1) the direct generation within ∼100−200 ps of relatively large nanoparticles with diameters ranging from ∼2.5 to 4 nm and (2) the much more gradual growth of smaller nanoparticles formed by agglomeration and coalescence of atomic clusters on the timescale of tens of nanoseconds. These two pathways are responsible for the early appearance of a bimodal mass-weighted particle size distribution.

IX. CROSSING INTERFACES

A. The discharge-liquid barrier

The discharge-liquid interface is very difficult to probe but interesting results could be obtained thanks to original experimental works. Sano *et al.*[284] recorded under microgravity conditions the development of an arc discharge submerged in water. They notice, from images of the reactor falling freely in a column under vacuum for about 4 s, that a transparent gas film was generated in the gas phase zone adjacent to the gas–liquid interface. The authors concluded that chemical reactions involving water were possible inside the bubble and not only at the water-gas interface.

The behaviour of nanoparticles in discharge bubbles is much better understood thanks to recent results obtained with synchrotron facilities on pulsed laser ablation in liquid.[285–287] It has been shown, with SAXS experiments, that the bubble interface is a quite impervious boundary for the primary and secondary particles. In PLAL, they cross the interface barrier by jet-like emission after the collapse of the first rebound. These two statements must also apply for submerged discharges created between two electrodes. Indeed, bubbles oscillations produce many different kinds of instabilities like Rayleigh-Taylor, Kelvin-Helmholtz, Landau-Darrieus or Birkhoff, leading to jet-like emission (**Fig. 14**).[288]

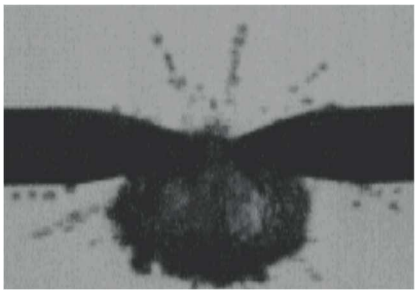

Fig. 14: Example of jet-like emission after the collapse of the first rebound of a bubble formed by nanosecond-pulsed discharge in heptane. Jets fragment into groups of aligned bubbles forming threads that point toward the center of the interelectrode gap.

Basically, the discharge-liquid barrier is rather nanoparticles tight. The transfer from one phase to the other is limited. This is also the case of the liquid-air barrier.

B. The liquid-air barrier and safety aspects

Sano *et al.*[38,289] synthesized carbon nanomaterials by erosion of graphite electrodes submerged in water. They noticed that nanoonions (average diameter : 25-30 nm) were majorly present as floating powder on the water surface, the other nanocarbons being rather found located on the bottom of the vessel.

Even though the liquid evaporates, this mechanism does not transport any nanoparticles in air.[290] This is why the dewetting of a colloidal dispersion concentrates nanoparticles at the moving front of the liquid fingers that form upon demixing of the two phases.[291] However, evaporation is affected by the presence of nanoparticles.[292]

As long as nanoparticles are left in the liquid, nanofluids in containers can be considered as safe. However, they also face public concerns about their safety in use as they can be spilled by accident. The lack of legal framework for their handling and recycling is a key issue.[293] It would be prudent to pursue green designs by choosing nontoxic or biodegradable nanoparticles.[294]

X. POST-TREATMENT WITH DISCHARGES AND ELECTRIC FIELD

Discharges in liquids or in contact with liquids can be used for appropriate post-treatments of colloidal dispersions. Sometimes, one-dimensional objects are also synthesized together with nanoparticles as their assembly can be driven by electric fields. Then, applying electric fileds with proper strengths in a post-treatment is a way to form new one-dimensional objects.

A. Post-treatment with discharges

1. Surface functionalization by atmospheric plasmas in contact with colloids

Because of the difficulty to control the complex chemistry induced by the presence of additives in processes using submerged discharges, it is possible to resort to a plasma post-treatment, as developed by Mariotti *et al.*[48] It relies on the utilization of plasma jets in contact with liquids. In this configuration,

electrons are injected into the liquid solution from the plasma phase. More efficiently than radicals formed in the gas phase and ultra-violet radiation, electrons are supposed to mainly contribute to a specific liquid chemistry for the surface engineering of pre-synthesized nanomaterials.

This post-processing results in considerable improvements in the stability of a colloidal dispersion, especially in the case of silicon nanocrystals in ethanol or water, which could not be observed with standard electrochemistry,[295] and carbon.[286] Stable Si-ncs can be created with different surface functional groups. This physicochemical change affects the optical properties of the colloid, its photoluminescence emission varying from 590 nm up to 650 nm just by changing the oxygen-bonding configuration at the surface.[297]

2. Post-treatments by discharges in liquids

Discharges in liquids can be used to activate physicochemical processes, for example by enhancing the reactivity of metal particles. High-voltage electrical discharges in liquids[74] are capable of:

- modifying the kinetics of reaction between particles;
- decreasing the energy of formation of new phases and compounds;
- increasing surface and bulk diffusion of reacting compounds;
- modifying the morphology and the dimensional characteristics;
- changing physical and mechanical properties of treated materials.

If these effects have been demonstrated, they are not very well documented and still to be investigated in detail. Nonetheless, these empirical post-treatments demonstrate clearly that discharges in liquids are also very promising for controlled modifications of nanoparticles and not only for their synthesis.

B. Role of electric fields on particles

A particle moving in a liquid environment can be submitted to many contributions like gravity, van der Waals or multi-body interactions, electrothermal flows, Brownian motion, fluid dynamics, etc. In this work, because light is shed on discharges produced between submerged electrodes, a special attention is paid to the electrokinetic motion of particles lying in an electrolyte exposed to an externally applied electric field.

1. Electro-osmosis

Electro-osmosis is responsible for the flow driven by the Coulomb force induced by an electric field on the net charge in the electrical double layer at the electrodes. Upon experiencing an electrical potential gradient, the mobile ions in the Gouy-Chapman layer move past the electrode surface and drag molecules of the solution, putting the fluid in motion. Nanoparticles, whatever their charge, are carried by the flow of the liquid and not because of their own electrical double layer.

The electro-osmotic flow is evaluated by solving the Navier-Stokes continuity and momentum equations coupled with Laplace's equation for the external electric field and Poisson's equation for the potential within the electric double layer.

Electro-osmosis exerts a long-range interaction and does not scale with the particle radius, contrary to dielectrophoresis (see next paragraph) that results from short-range interactions and scales with the particle volume. Both forces can be combined to trap and manipulate nanoparticles.[298]

The principal drawback with DC electro-osmosis is the need for high DC voltages (up to 1 kV across a 1 cm gap typically to reach acceptable flow velocities (around 100 μm s^{-1}).[299] This can lead to unwanted electrochemical reactions, electrode dissolution, gas bubble production and/or hydrodynamic instability. Resorting to AC electro-osmosis with voltages of only a few volts by using planar periodic arrays of interdigitated, asymmetric electrodes can overcome these drawbacks.

It was shown by Gierhart *et al.*[300] that particle motion by AC electro-osmosis greatly influences the morphology of resultant nanoparticle assemblies.[301] With frequencies ranging typically from 0.1 to 10 kHz, this phenomenon is likely to be considered in AC-excited submerged discharges (see **Table 1**).

2. Electrophoresis (EP)

The motion of a submicron particle is influenced by the cloud of ions near the charged or polarised particle induced by the external electric field.

The particle can be initially charged and possess an equilibrium surface charge, which need not be uniformly distributed over its surface. The interaction between the electric field and the surface charge corresponds to the linear EP problem, where the dynamic reaction experienced by the particle and the induced mobility are linear in the external electric field.

For a polarisable uncharged particle, the external electric field produces an additional space charge distribution in the electrolyte which decays away from the particle. The corresponding induced-charge electrophoresis (ICEP) problem implies that the force and torque experienced by the particle are nonlinear (quadratic) in the electric field.

3. Dielectrophoresis (DEP)

Dielectrophoresis can be utilized to assemble nanoparticles into wires. Alternating current fields allow assembly of particles without the interference of direct current effects like electro-osmotic and electrochemical effects. The dielectrophoretic force results from the interaction of particle dipoles in a non-uniform DC or AC field. It is conservative and oriented along the field gradient:

$$\vec{F}_{dep}^{\,cons} = 2\pi a^3 \varepsilon_m \Re(\omega) \cdot \vec{\nabla} \left| \vec{E}_{rms} \right|^2 \tag{15}$$

a is the particle radius,. $\Re$ denotes the real part of the Clausius–Mossotti factor, which is an effective polarisability of the particle in the medium, and it depends on ω, the angular field frequency. It is expressed by the complex relative permittivities of the particle $\tilde{\varepsilon}_p$ and of the medium $\tilde{\varepsilon}_m$:

$$\Re = \Re e\left(\frac{\tilde{\varepsilon}_p(\omega)-\tilde{\varepsilon}_m}{\tilde{\varepsilon}_p(\omega)+2\tilde{\varepsilon}_m}\right) \tag{16}$$

$\Re$ is bounded between −1/2 and 1 and varies with the frequency of the applied field and the complex permittivity of the medium. $\vec{\nabla}\left|\vec{E}_{rms}\right|^2$ is the gradient of the square of the root-mean-square electrical field. Then, the strength of the force exerted on a particle depends on $\vec{\nabla}\left|\vec{E}_{rms}\right|^2$ and also on $\Re$. The frequency dependence of $\Re$ is given by:

$$\Re = \left(\frac{\varepsilon_p(\omega)-\varepsilon_m}{\varepsilon_p(\omega)+2\varepsilon_m}\right) + \frac{3\left(\varepsilon_m\sigma_p-\varepsilon_p\sigma_m\right)}{\tau_{MW}\left(\sigma_p+2\sigma_m\right)^2\left(1+\omega^2\tau_{MW}^2\right)} = \Re_\infty + \left(\Re_0-\Re_\infty\right)\left(1+\omega^2\tau_{MW}^2\right)^{-1} \tag{17}$$

At high frequency, when $\omega >> \tau_{MW}^{-1} = \frac{\sigma_p+2\sigma_m}{\varepsilon_p+2\varepsilon_m}$ where σ_m denotes the electric conductivity,[302] $\Re \to \Re_\infty = \left(\frac{\varepsilon_p(\omega)-\varepsilon_m}{\varepsilon_p(\omega)+2\varepsilon_m}\right)$. At low frequency, $\Re \to \Re_0 = \left(\frac{\sigma_p(\omega)-\sigma_m}{\sigma_p(\omega)+2\sigma_m}\right)$

Positive dielectrophoresis occurs when $\Re > 0$; the force is in the direction of increasing field strength and the particles are attracted by the electrode edges. The opposite behavior is observed for negative values.

In the interelectrode gap, nanoparticles experience a large electric field that induces a dipole in each of them if they are not conductors. In the case of most metallic particles for instance, $\Re = 1$ because the conduction band electrons redistribute continually to annul the internal electric field. The field frequency needed to keep charges separated on each side of a metallic nanoparticle should excess tens of THz. On the contrary, dielectric nanoparticles with diameters between 10 nm and 100 nm can be trap by an ac field in the MHz range.[303]

However, in 2001, Hermanson *et al.*[304] succeeded in synthesizing gold wires with millimeter length in an AC electric field from a suspension of gold nanoparticles by dielectrophoresis. They suggested some collective effect or complex electrohydrodynamic interactions to account for direct chaining of gold nanoparticles.

Barsotti *et al.*[305] considered in addition to the dipole contribution to the DEP force, effects of higher-order polarisation moments and forces.[306] These higher-order corrections to the DEP force cannot be

neglected for conductive particles in AC fields and introduce a non-conservative term proportional to the curl of the vector electromechanical potential $\vec{W}_n$ and the imaginary part of Clausius–Mossotti factor.

$$\vec{F}_{dep}^{\,non-cons} = 2\pi a^3 \varepsilon_m \Im(\omega) \cdot \vec{\nabla} \times \vec{W}_n \tag{18}$$

4. Dipolophoresis (DPP)

In the general case where spatially non-uniform electric fields are encountered, both DEP and ICEP contribute to the particle movement. The combined non-linear electrokinetic effect is known as dipolophoresis.[307] DEP and ICEP mechanisms act in different directions and their combination can either be additive or subtractive. Under appropriate circumstances like a constant gradient field, the sum of the two contributions can be null and particle mobility turned to zero.

XI. OUTLOOK AND NEW APPLICATIONS

In this pedagogical review, emphasis is put on specificities of discharges in liquids in nanoparticles' synthesis. As colloids and nanofluids are generated by these processes, application related to these biphasic systems is extremely large. For instance, they can be used:

- to replace water and ethylene glycol as conventional coolants in an automotive car radiator;[308]
- to produce hydrogen via their use as working fluid in solar parabolic trough collectors;[309]
- to recover oil more efficiently in rock pores by depositing a wedge film making rock surfaces more dewettable;[310]
- to decrease by several orders of magnitude bacterial activity including Gram-negative, Gram-positive and spore bacteria;[311]
- to serve as a new reaction media in the preparation of chemicals, like amides via direct amidation of aliphatic carboxylic acids;[312]
- to enable sensing like, for instance, those magnetically polarizable nanoemulsions used for imaging internal defects in materials;[313] etc.

There is a number of challenges that deserve to be tackled:

- Recently, nanoalloys, *i.e.* single solid solution, made of immiscible elements have been synthesized by PLAL.[314,315] Producing them by discharges in liquids has been showed to be possible too.[316] Mechanisms leading to nanoalloying of immiscible elements are still to be clarified.

These new results open up the way to the study of optical properties of metallic nanoalloys.[315,317] Engineering of nanoalloys for optical properties consists in controlling defects, element distributions, oxidation and surface functionalization processes.

- Chemistry driven by discharges in liquids is a very complex topic, still in its infancy. Discharges in carbonaceous liquids for instance are responsible for the deposit of a carbon layer onto nanoparticles, but they also produce unusual chemical by-products like polyynes.[318] This is also true for the synthesis of uncommon nitrogen polymer[319] or diamondoids.[320]

Chemistry driven by discharges in liquids is extremely complex and capable of producing rare by-products. The possibility of a better control of chemical reactions in the liquid phase is an important stake. It is a major challenge for discharges in contact with liquids[321] but also for discharges in liquids.

- Multimodal size distributions are still an issue for large scale production of well-controlled nanoparticles but huge progress made recently on erosion mechanisms gives promising outlook to achieve unimodal monodisperse size distributions.

The possibility of controlling size distributions in a one-step process is not an easy task. If unimodal distributions have been produced by several groups (see **Table 1**), none of them achieved to get monodisperse distributions. Discharges in liquids containing precursors are more suited to this goal than processes based on electrodes erosion.

- Control of defects to control properties.

Engineering of defects (twin defects, vacancies, edges, doping, etc.) in nanoparticles is a key topic to better control optical[322] and catalytic properties.[323] Controlling defects in nanoparticles by discharges in liquids remains hitherto a dare to take. This is could be a way to develop low-cost catalysts based on non-rare chemical elements or to tune non-linear effects in nanoparticles for optics.

- Control of surface physicochemical states.

Controlling the grafting of selected chemical functional groups on nanoparticles remains a challenge. It is essential anyway to set the stability of nanoparticles in colloidal dispersion. It also control their activity, not only catalytically but also optically. It may even affect the chemical homogeneity of very small nanoparticles. As seen before, discharge-enhanced post-treatments can be used to functionalize nanoparticles, but resorting to these processes cannot be generalized to any situation.

ACKNOWLEDMENTS

The authors acknowledge the French PIA (programme d'investissements d'avenir) project Lorraine Université d'Excellence (Ref. ANR-15-IDEX-04-LUE) for financial support.

DATA AVAILABLITY STATEMENTS FOR AUTHOR USE

Data available on request from the authors

BIBLIOGRAPHY

[1]H. Fizeau and L. Foucault, C. R. Acad. Hebd. Seances Acad. Sci. **18**, 746 and 860 (1844).

[2]J. Gubkin, Annal. Physik Lpz **268**, 114 (1887).

[3]A. Hickling and G. R. Newns, Proc. Chem. Soc. London **11**, 368 (1959).

[4]K. Klüpfel, Annalen der Phys. Lpz **321**, 574 (1905).

[5]A. Makowetsky, Z. Elektrochem. **17**, 217 (1911).

[6]V. Y. Ushakov, V. F. Klimkin and S. M. Korobeynikov, Impulse breakdown of liquids. Springer Science & Business Media. (2007).

[7]K. Harada and T. Iwasaki, Nature **250**, 426 (1974). See also K. Harada and S. Suzuki, Nature **266**, 275 (1977)

[8]H. H. Kellogg, J Electrochem. Soc. **97**, 133 (1950).

[9]A. Hickling and G. R. Newns, J. Chem. Soc. (Resumed) **1024**, 5177 (1961).

[10]A. Hickling and M. Ingram, J. Electroanal. Chem. **8**, 65 (1964). See also A. Hickling, Electrochemical processes in glow discharge at the gas-solution interface. In Modern Aspects of Electrochemistry **6**, pp. 329-373. Springer, Boston, MA. (1971).

[11]S. Webzell, Machin. Prod. Eng. **159**, 41 (2001).

[12]V. N. Gusseff, Method and apparatus for the electrolytic treatment of metals. British Patent, 335003A (1930).

[13]A. H. Meleka and D. A. Glew, Int. Metals Rev. **22**, 229 (1977).

[14]K. H. Ho and S. T. Newman, J Machine Tools Manufact. **43**, 1287 (2003).

[15]E. Nairne, Phil. Trans. Royal Soc. London **64**, 79 (1774).

[16]R. Abrams, Production and Analysis of Radioactive Aerosols, CH3629 (University of Chicago, Chicago, Illinois, 1946).

[17]G. S. Sarkisov, P. V. Sasorov, K. W. Struve and D. H. McDaniel, J. Appl. Phys. **96**, 1674 (2004).

[18]M. J. Joncich and D. C. Reu, Synthesis of inorganic binary compounds using exploding wire techniques. In: Chace W.G. and More H.K. eds. Exploding Wires, Vol. 3. Proc. of the 3rd Conf. on Exploding Wire Phenomenon. Boston, USA, 10–12 March 1964, Plenum Press, New York, pp. 353–359 (1964).

[19]S. V. Lebedev and A. I. Savvatimskiĭ, Sov. Phys. Uspekhi **27**, 749 (1984).

[20]Y. E. Krasik, A. Grinenko, A. Sayapin, S. Efimov, A. Fedotov, V. Z. Gurovich, and V. I. Oreshkin, IEEE Trans. Plasma Sci. **36**, 423 (2008).

[21]D. Veksler, A. Sayapin, S. Efimov and Y. E. Krasik, IEEE Trans. Plasma Sci. **37**, 88 (2008).

[22]Y. A. Kotov, J. Nanopart. Res. **5**, 539 (2003).

[23]C. Cho, Y. W. Choi, C. Kang and G. W. Lee, Appl. Phys. Lett. **91**, 141501 (2007).

[24]V. Y. Dolmatov, M. V. Veretennikova, V. A. Marchukov and V. G. Sushchev, Phys. Solid State **46**, 611 (2004).

[25]V. V. Danilenko, Phys. Solid State **46**, 595 (2004).

[26]T. H. Maiman, Nature **187**, 493 (1960).

[27]H. M. Smith and A. F. Turner, Appl. Opt. **4**, 147 (1965).

[28]P. P. Patil, D. M. Phase, S. A. Kulkarni, S. V. Ghaisas, S. K. Kulkarni, S. M. Kanetkar, S. B. Ogale and V. G. Bhide, Phys. Rev. Lett. **58**, 238 (1987).

[29]M. DiDomenico Jr, J. Appl. Phys. **35**, 2870 (1964).

[30]L. E. Hargrove, R. L. Fork and M. A. Pollack, Appl. Phys. Lett. 5, 4 (1964).

[31]R. L. Fork, B. I. Greene and C. V. Shank, Appl. Phys. Lett. **38**, 671 (1981).

[32]K. C. Phillips, H. H. Gandhi, E. Mazur and S. K. Sundaram, Adv. Opt. Photon. **7**, 684 (2015).

[33]H. Zeng, X. W. Du, S. C. Singh, S. A. Kulinich, S. Yang, J. He and W. Cai, Adv. Funct. Mater. **22**, 1333 (2012).

[34]W. Ishibashi, T. Araki, K. Kishimoto and H. Kuno, Ceram. Jpn **6**, 461 (1971).

[35]A. G. Dubovoy, A. E. Perekos and K. V. Chuistov, Phys. Metals **6**, 1085 (1985).

[36]T. Sato, K. Usuki, A. Okuwaki and Y. Goto, J. Mater. Sci. **27**, 3879 (1992).

[37]M. Ishigami, J. Cumings, A. Zettl and S. Chen, Chem. Phys. Lett. **319**, 457 (2000).

[38]N. Sano, H. Wang, M. Chhowalla, I. Alexandrou and G. A. J. Amaratunga, Nature **414**, 506 (2001).

[39]S. Dadras, P. Jafarkhani, M. J. Torkamany and J. Sabbaghzadeh, J. Phys. D: Appl. Phys. **42**, 025405 (2009).

[40]V. S. R. Murthy and P. K. Philip, Int. J. Mach. Tools Manu. **27**, 469-477 (1987).

[41]D. Kremer, J. L. Lebrun, B. Hosari and A. Moisan, CIRP Annals **38**, 199-202 (1989).

[42]I. Gyo Koo, M. Seok Lee, J. Hee Shim, J. Hwan Ahn and W. Moo Lee, J. Mater. Chem. **15**, 4125 (2005).

[43]Y. Shimizu, T. Sasaki, T. Ito, K. Terashima and N. Koshizaki, J. Phys. D: Appl. Phys. **36**, 2940 (2003).

[44]K. Furuya, Y. Hirowatari, T. Ishioka and A. Harata, Chem. Lett. **36**, 1088 (2007).

[45]C. Richmonds and R. M. Sankaran, Appl. Phys. Lett. **93**, 131501 (2008).

[46]H. Furusho, K. Kitano, S. Hamaguchi and Y. Nagasaki, Chem. Mater. **21**, 3526 (2009).

[47]P. Bruggeman and C. Leys, J. Phys. D: Appl. Phys. **42**, 053001 (2009).

[48]D. Mariotti, J. Patel, V. Švrček and P. Maguire, Plasma Process. Polym, **9**, 1074 (2012).

[49]K. C. Kao, Brit. J. Appl. Phys. **12**, 629 (1961).

[50]I. E. Balygin, Electric Strength of Liquid Dielectrics, Izd. Energiya, (Moscow-Leningrad, in Russian, 1964).

[51]C. Yamabe, K. Horii and E. Sakai, Proceedings of the 2nd Annual Conference on Ozone Science and Technology in Japan. pp. 163-166 (in Japanese - 1993)

[52]J. G. Shin, C. S. Park, H. J. Kim, D. S. Kum, E. Y. Jung, G. T. Bae, H. J. Jang, J. Y. Kim, B.-G. Cho, B. J. Shin and H. S. Tae, Molec. Cryst. Liquid Cryst. **678**, 20 (2019).

[53]M. Yamada, Wahyudiono, S. Machmudah, H. Kanda, Y. Zhao and M. Goto, ACS Omega **5**, 17679 (2020).

[54]S. Atzeni and J. Meyer-ter-Vehn, The Physics of Inertial Fusion: Beam-Plasma Interaction, Hydrodynamics, Hot Dense Matter, **125** (OUP Oxford. 2004).

[55]Max Ulrich Schoop, Patent n°AT1285. Elektrolytischer Wasserzersetzungs-Apparat. (Appl. Date: 1899-07-13).

[56]S. Siegmann and C. Abert, Surf. Coat. Technol. **220**, 3 (2013).

[57]R. B. Heimann, Plasma-spray coating: principles and applications, John Wiley & Sons (2008).

[58]G. I. Taylor, Proc. Royal Soc. London. A. Math. Phys. Sci. **280**, 383 (1964).

[59]D. B. Hager and N. J. Dovichi, Anal. Chem. **66**, 1593 (1994).

[60]O. V. Kim and P. F. Dunn, Langmuir **26**, 15807 (2010).

[61]F. Q. Zhao, M. C. Lai and D. L. Harrington, SAE Trans., 861 (1997).

[62]P. Tardiveau and E. Marode, J. Phys. D: Appl. Phys. **36**, 1204 (2003).

[63]L. J. Ward, W. C. E. Schofield, J. P. S. Badyal, A. J. Goodwin and P. J. Merlin, Chem. Mater. **15**, 1466 (2003).

[64]F.Massines, C. Sarra-Bournet, F. Fanelli, N. Naudé and N. Gherardi, N. (2012). Plasma Process. Polym. **9**, 1041.

[65]F. Fanelli, A.M. Mastrangelo and F. Fracassi, Langmuir **30**, 857 (2014).

[66]J. Profili, S. Dap, O. Levasseur, N. Naude, A. Belinger, L. Stafford and N. Gherardi, J. Phys. D: Appl. Phys. **50**, 075201 (2017).

[67]I. Nakatani, T. Furubayashi, T. Takahashi and H. Hanaoka, J. Magn. Magn. Mater. **65**, 261 (1987).

[68]T. Torimoto, K. I. Okazaki, T. Kiyama, K. Hirahara, N. Tanaka and S. Kuwabata, Appl. Phys. Lett. **89**, 243117 (2006).

[69]A. Imanishi, M. Tamura and S. Kuwabata, Chem. Comm. **13**, 1775 (2009).

[70]A. A. Sin'kevich and Y. A. Dovgalyuk, Radiophys. Quant. Electr. **56**, 818 (2014).

[71]R. Navarro-González and S. I. Ramírez, Adv. Space Res. **19**, 1121 (1997).

[72]N. Arora and N. N. Sharma, N. N. Diam. Relat. Mater. **50**, 135 (2014).

[73]T. Belmonte, A. Hamdan, F. Kosior, C. Noël and G. Henrion, J. Phys. D: Appl. Phys. **47**, 224016 (2014).

[74]V. S. Burakov, E. A. Nevar, M. I. Nedel'Ko and N. V. Tarasenko, Russ. J. Gen. Chem. **85**, 1222 (2015).

[75]Y. A. Lebedev, High Temp. 56, 811 (2018).

[76]T. Morishita, T. Ueno, G. Panomsuwan, J. Hieda, A. Yoshida, M. A. Bratescu and N. Saito, Sci. Rep. **6**, 36880 (2016).

[77]K. K. Ostrikov, U. Cvelbar and A. B. Murphy, J. Phys. D: Appl. Phys. **44**, 174001 (2011).

[78]G. Saito and T. Akiyama, J. Nanomater. **2015** (2015).

[79]N. Saito, M. A. Bratescu and K. Hashimi, Jap. J. Appl. Phys. **57**, 0102A4 (2018).

[80]P. Vanraes and A. Bogaerts, Appl. Phys. Rev. **5**, 031103 (2018).

[81]A. Voloshko and T. E. Itina, Nanopart. Technol., Ed. by M. Aliofkhazraei, IntechOpen, 1-12 (2015).

[82]X. Ye and C. M. Wai, J. Chem. Educ. **80**, 198 (2003).

[83]T. Yonezawa, D. Čempel and M. T. Nguyen, Bull. Chem. Soc. Jap. **91**, 1781 (2018).

[84]P. J. Bruggeman *et al.*, Plasma Sources Sci. Technol. **25**, 053002 (2016).

[85]V. S. Burakov, V. V. Kiris, M. I. Nedelko, N. N. Tarasenka, A. A. Nevar and N. V. Tarasenko, Eur. Phys. J. Appl. Phys. **79**, 10801 (2017).

[86]Q. Chen, J. Li and Y. Li, J. Phys. D: Appl. Phys. **48**, 424005 (2015).

[87]S. K. S. Gupta, Plasma Sources Sci. Technol. **24**, 063001 (2015).

[88]S. K. S. Gupta, Plasma Chem. Plasma Process. **37**, 897 (2017).

[89]S. Horikoshi and N. Serpone, RSC Adv. **7**, 47196 (2017).

[90]T. Kaneko, K. Baba and R. Hatakeyama, Plasma Phys. Control. Fusion **51**, 124011 (2009).

[91]T. A. Kareem and A. A. Kaliani, Ionics **18**, 315 (2012).

[92]N. K. Kaushik, N. Kaushik, N. N. Linh, B. Ghimire, A. Pengkit, J. Sornsakdanuphap, S.-J. Lee and E. H. Choi, Nanomater. **9**, 98 (2019).

[93]L. Lin and Q. Wang, Plasma Chem. Plasma Process. **35**, 925 (2015).

[94]D. Mariotti and R. M. Sankaran, J. Phys. D: Appl. Phys. **43**, 323001 (2010).

[95]F. Rezaei, P. Vanraes, A. Nikiforov, R. Morent and N. De Geyter, Materials **12**, 2751 (2019).

[96]P. Rumbach and D. B. Go, Topics Catal. **60**, 799 (2017).

[97]V. Amendola and M. Meneghetti, Phys. Chem. Chem. Phys. **15**, 3027 (2013).

[98]A. Kanitz, M. R. Kalus, E. L. Gurevich, A. Ostendorf, S. Barcikowski and D. Amans, Plasma Sources Sci. Technol. **28**, 103001 (2019).

[99]P. Liu, H. Cui, C. X. Wang and G. W. Yang, Phys. Chem. Chem. Phys. **12**, 3942 (2010).

[100]S. V. Rao, G. K. Podagatlapalli and S. Hamad, J. Nanosci. Nanotechnol. **14**, 1364 (2014).

[101]E. Stratakis, Sci. Adv. Mater. **4**, 407 (2012).

[102]J. Xiao, P. Liu, C. X. Wang and G. W. Yang, Prog. Mater. Sci. **87**, 140 (2017).

[103]Z. Yan and D. B. Chrisey, J. Photochem. Photobiol. C: Photochem. Rev. **13**, 204 (2012).

[104]G. W. Yang, Prog. Mater. Sci. **52**, 648 (2007).

[105]E. Brinley, K. S. Babu and S. Seal, Jom, **59**, 54 (2007).

[106]P. Fauchais, R. Etchart-Salas, V. Rat, J. F. Coudert, N. Caron and K. Wittmann-Ténèze, J. Therm. Spray Technol. **17**, 31 (2008).

[107]E. H. Jordan, C. Jiang and M. Gell, J. Therm. Spray Technol. **24**, 1153 (2015).

[108]J. Karthikeyan, C. C. Berndt, J. Tikkanen, S. Reddy and H. Herman, Mater. Sci. Eng. A **238**, 275 (1997).

[109]F. Palumbo, C. L. Porto, F. Fracassi and P. Favia, Coatings **10**, 440 (2020).

[110]A. Stancampiano, T. Gallingani, M. Gherardi, Z. Machala, P. Maguire, V. Colombo, J.-M. Pouvesle and E. Robert, Appl. Sci. **9**, 3861 (2019).

[111]H. Shi, J. Wu, X. Li, A. B. Murphy, X. Li, C. Li and P. Li, Plasma Sources Sci. Technol. **28**, 085010 (2019).

[112]P. Anantha, T. Cheng, Y. Y. Tay, C. C. Wong and R. V. Ramanujan, Nanoscale **7**, 16812 (2015).

[113]C. Janiak, Z. Naturforsch. B **68**, 1059 (2013).

[114]M. T. Nguyen and T. Yonezawa, Sci. Technol. Adv. Mater. **19**, 883 (2018).

[115]M. V. Novikov, L. D. Kisterska, V. V. Sadokhin, V. P. Sadokhin and V. M. Perevertailo, Powder Metal. Metal Ceram. **51**, 26 (2012).

[116]H. Wender, R. V. Gonçalves, A. F. Feil, P. Migowski, F. S. Poletto, A. R. Pohlmann, J. Dupont and S. R. Teixeira, J. Phys. Chem. C **115**, 16362 (2011).

[117]H. Wender, P. Migowski, A. F. Feil, S. R. Teixeira and J. Dupont, Coord. Chem. Rev. **257**, 2468 (2013).

[118]*Laser Precision Microfabrication*. Ed. by K. Sugioka, M. Meunier and A. Piqué. Springer Series in Materials Science, vol 135. Springer, Berlin, Heidelberg (2010).

[119]*Plasma chemistry and catalysis in gases and liquids*, Ed. by V. I. Pârvulescu, M. Magureanu and P. Lukes. John Wiley & Sons. (2012).

[120]*Corona Discharge Micromachining for the Synthesis of Nanoparticles: Characterization and Applications*, Ed. by .R. K. Sahu and S. S. Hiremath. CRC Press. (2019).

[121]J. Siegel, A. Řezníčková, P. Slepička and V. Švorčík, Nanopart. Technol. **73**, (2015).

[122]*Laser ablation in liquids: principles and applications in the preparation of nanomaterials*. Ed. by G. Yang. CRC Press. (2012).

[123]P. K. Karahaliou, P. Svarnas, S. N. Georga, N. I. Xanthopoulos, D. Delaportas, C. A. Krontiras and I. Alexandrou, J. Nanopart. Res. **14**, 1297 (2012).

[124]D. Bera, G. Johnston, H. Heinrich and S. Seal, Nanotechnol. **17**, 1722 (2006).

[125]Z. E. Horváth, K. Kertész, L. Pethő, A. A. Koós, L. Tapasztó, Z. Vértesy, Z., Z. Osváth, Al. Darabont, P. Nemes-Incze, Zs. Sárközi and L. P. Biró, Curr. Appl. Phys. **6**, 135-140 (2006).

[126]D. Bera, E. Brinley, S. C. Kuiry, M. McCutchen, S. Seal, H. Heinrich and B. Kabes, Rev. Sci. Instrum. **76**, 033903 (2005).

[127]M. Trad, A. Nominé, N. Tarasenka, J. Ghanbaja, C. Noël, M. Tabbal and T. Belmonte, Front. Chem. Sci. Eng. **13**, 360 (2019).

[128]K. H. Tseng, H. L. Lee, C. Y. Liao, K. C. Chen and H. S. Lin, J. Nanomat. **2013**. (2013).

[129]B. Rebollo-Plata, M. P. Sampedro, G. Gallardo-Gómez, N. Ortega-Miranda, C. F. Bravo-Barrera, G. Daniel-Pérez, B. Zenteno-Mateo, D. Hernandez-Cruz and S. Jiménez-Sandoval, Revista Mexicana Física **60**, 227 (2014).

[130]A. A. Ashkarran, S. M. Mahdavi, M. M. Ahadian and M. R. H. Nezhad, Appl. Phys. A **96**, 423 (2009).

[131]A. A. Ashkarran, Plasma Sci. Technol. **15**, 376 (2013).

[132]S. Bhattacharyya, D. Staack, E. A. Vitol, R. Singhal, A. Fridman, G. Friedman and Y.Gogotsi, Adv. Mater. **21**, 4039-4044 (2009).

[133]H. Ghomi, M. Yousefi, N. Shahabi and M. Khoramabadi, Radiat. Effects Defects Solids **168**, 881 (2013).

[134]Y. K. Heo, S. M. Kim and S. Y. Lee, Phys. Script. **T139**, 014025 (2010).

[135]J. Hieda, N. Saito and O. Takai, J. Vac. Sci. Technol. A **26**, 854 (2008).

[136]J. K. Lung, J. C. Huang, D. C. Tien, C. Y. Liao, K. H. Tseng, T. T. Tsung, W. S. Kao, T. H. Tsai, C. S. Jwo, H. M. Lin and L. Stobinski, J. Alloys Comp. **434**, 655 (2007).

[137]D. C. Tien, L. C. Chen, N. Van Thai and S. Ashraf, J. Nanomater. **2010**, (2010).

[138]S. Sulaimankulova, A. Mametova and Z. Abdullaeva, SN Appl. Sci. **1**, 1427 (2019).

[139]K. H. Tseng, J. C. Huang, C. Y. Liao, D. C. Tien and T. T. Tsung, J. Alloys Comp. **472**, 446 (2009).

[140]H. Kabbara, J. Ghanbaja, C. Noël and T. Belmonte, Mater. Chem. Phys. **217**, 371 (2018).

[141]H. Kabbara, J. Ghanbaja, C. Noël and T. Belmonte, Mater. Chem. Phys. **207**, 350 (2018).

[142]X. Hu, X. Zhang, X. Shen, H. Li, O. Takai and N. Saito, Plasma Chem. Plasma Process. **34**, 1129 (2014).

[143]C. H. Lo, T. T. Tsung, L. C. Chen, C. H. Su and H. M. Lin, J. Nanopart. Res. **7**, 313 (2005).

[144]P. Pootawang, N. Saito and S. Y. Lee, Nanotechnol. **24**, 055604 (2013).

[145]W. T. Yao, S. H. Yu, Y. Zhou, J. Jiang, Q. S. Wu, L. Zhang and J. Jiang, J. Phys. Chem. B **109**, 14011 (2005).

[146]L. C. Chen and S. H. Pai, Mater. Trans. **45**, 3071 (2004).

[147]V. Eskizeybek, O. Demir, A. Avci and M. Chhowalla, J. Nanopart. Res. **13**, 4673 (2011).

[148]A. Hamdan, H. Kabbara, C. Noel, J. Ghanbaja, A. Redjaïmia and T. Belmonte, Particuology **40**, 152 (2018).

[149]N. Parkansky, B. Alterkop, R. L. Boxman, S. Goldsmith, Z. Barkay and Y. Lereah, Powder Technol. **150**, 36 (2005).

[150]M. Trad, A. Nominé, C. Noël, J. Ghanbaja, M. Tabbal and T. Belmonte, Plasma Proc. Polym. **17**, 1900255 (2020).

[151]Y. Mizukoshi, F. Hori and K. Okitsu, Jap. J. Appl. Phys. **57**, 0102A5 (2017).

[152]N. A. Bulychev, M. A. Kazaryan, L. S. Lepnev, A. S. Averyushkin, E. A. Morosova, A. Y. Stavtsev and A. A. Chernov, Instrum. Exp. Tech. **59**, 842 (2016).

[153]P. Vanraes, A. Y. Nikiforov and C. Leys, Electrical discharge in water treatment technology for micropollutant decomposition. Plasma science and technology-progress in physical states and chemical reactions (Chap. 15), Ed. by Tetsu Mieno, pp 429-478 (2016).

[154]A. Hamdan, J. N. Audinot, S. Migot-Choux, C. Noel, F. Kosior, G. Henrion and T. Belmonte, Adv. Eng. Mater. **15**, 885 (2013).

[155]T. Shizuno, H. Miyazoe, K. Saito, S. Stauss, M. Suzuki, T. Sasaki and K. Terashima, Jap. J. Appl. Phys. **50**, 030207 (2011).

[156]N. Parkansky, B. A. Alterkop, R. L. Boxman, H. Mamane and D. Avisar, Plasma Chem. Plasma Process. **28**, 583 (2008).

[157]Z. Kozáková, F. Krčma, L. Čechová, S. Simic and L. Doskočil, Plasma Phys. Technol. **6**, 180 (2019).

[158]L. N. Shiyan, N. A. Yavorovskii, A. V. Pustovalov E. N. Gryaznova, IOP Conf. Series: Mater. Sci. Engin. Vol. 81: *Radiation-Thermal Effects and Processes in Inorganic Materials.* UK, 2015. (Vol. 81, p. 120775). IOP Publishing. (2015, April).

[159]M. Mardanian, A. A. Nevar, M. Nedel'ko and N. V. Tarasenko, Eur. Phys. J. D, **67**, 208 (2013).

[160]F. De Baerdemaeker, M. Monte and C. Leys, IEEE Trans. Plasma Sci. **33**, 492 (2005).

[161]D. D. DiBitonto, P. T. Eubank, M. R. Patel and M. A. Barrufet, J. Appl. Phys. **66**, 4095 (1989).

[162]A. Starikovskiy, Y. Yang, Y. I. Cho, and A. Fridman, Plasma Sources Sci. Technol. **20**, 024003 (2011).

[163]A. Hamdan, F. Kosior, C. Noel, G. Henrion, J. N. Audinot, T. Gries and T. Belmonte, J. Appl. Phys. **113**, 213303 (2013).

[164]R. Qotba, F. Aitken and A. Denat, Experimental investigation of the behavior of microscopic bubbles in insulating liquids: influence of pressure and temperature. In IEEE International Conference on Dielectric Liquids, 2005. ICDL 2005. (pp. 115-118). (June 2005).

[165]C. Wu and L. V. Zhigilei, Appl. Phys. A **114**, 11 (2014).

[166]C. Wu and L. V. Zhigilei, J. Phys. Chem. C **120**, 4438 (2016).

[167]H. G. Fan and R. Kovacevic, J. Phys. D: Appl. Phys. **37**, 2531 (2004).

[168]M. Ushio, M. Tanaka and J. J. Lowke, IEEE Trans. Plasma Sci. **32**, 108 (2004).

[169]J. J. Gonzalez, F. Cayla, P. Freton and P. Teulet, J. Phys. D: Appl. Phys. **42**, 145204 (2009).

[170]A. Hamdan, I. Marinov, A. Rousseau and T. Belmonte, J. Phys. D: Appl. Phys. **47**, 055203 (2014).

[171]X. Xu and D. A. Willis, J. Heat Transfer **124**, 293 (2002).

[172]T. DebRoy, S. Basu and K. Mundra, J. Appl. Phys. **70**, 1313 (1991).

[173]M. E. Povarnitsyn, T. E. Itina, P. R. Levashov and K. V. Khishchenko, Phys. Chem. Chem. Phys. **15**, 3108 (2013).

[174]C. Y. Shih, M. V. Shugaev, C. Wu and L. V. Zhigilei, J. Phys. Chem. C **121**, 16549 (2017).

[175]C. Y. Shih, M. V. Shugaev, C. Wu and L. V. Zhigilei, Phys. Chem. Chem. Phys. **22**, 7077 (2020).

[176]C.-Y. Shih, R. Streubel, J. Heberle, A. Letzel, M. V. Shugaev, C. Wu, M. Schmidt, B. Gökce, S. Barcikowski and L. V. Zhigilei, Nanoscale **10**, 6900 (2018).

[177]A. N. Volkov and L. V. Zhigilei, Int. J. Heat Mass Transfer **112**, 300 (2017).

[178]V. Sarou-Kanian, F. Millot, J.C. Rifflet, Int. J. Thermophys. **24**, 277 (2003).

[179]V. S. Ajaev and D. A. Willis, Phys. Fluids **15**, 3144 (2003).

[180]D. A. Willis and X. Xu, J. Heat Transfer 122 (2003) 763–769.

[181]A. Hassanein, V. Belan, I. Konkashbaev, L. Nikandrov, V. Safronov, A. Zhitlukhin and V. Litunovsky, J. Nucl. Mater. **241**, 288 (1997).

[182]M. Balden, V. Rohde, S. Lindig, A. Manhard, K. Krieger and A. U. Team, J. Nucl. Mater. **438**, S220 (2013).

[183]J.C. Bird, R. De Ruiter, L. Courbin and H. A. Stone, Nature **465**, 759 (2010).

[184]J. T. Holgate and M. Coppins, J. Phys. D: Appl. Phys. **53**, 105204 (2019).

[185]A. Hamdan, C. Noel, F. Kosior, G. Henrion and T. Belmonte, J. Appl. Phys. **113**, 043301 (2013).

[186]A. A. Kuchmizhak, A. V. Nepomnyashchii, O. B. Vitrik and Y. N. Kulchin, Phys. Procedia **86**, 66 (2017).

[187]P. Knotek and L. Tichy, Mater. Res. Bull. **48**, 3268 (2013).

[188]W. Luo, W. Hu, and S. Xiao, J. Phys. Chem. C **112**, 2359 (2008).

[189]Q. Zhang, J. Wang, S. Tang, Y. Wang, J. Li, W. Zho and Z. Wang, Phys. Chem. Chem. Phys. **21**, 4122 (2019).

[190]Y. Shu, T. Ando, Q. Yin, G. Zhou and Z. Gu, Nanoscale **9**, 12398 (2017).

[191]G. Radnóczi, E. Bokanyi, Z. Erdélyi and F. Misják, Acta Mater. **123**, 82 (2017).

[192]M. Zhang, J. G. Wen, M. Y. Efremov, E. A. Olson, Z. S. Zhang, L. Hu, L. P. de la Rama, R. Kummamuru, K. L. Kavanagh, Z. Ma and L. H. Allen, J. Appl. Phys. **111**, 093516 (2012).

[193]O. P. Pandey, S. N. Ojha and S. Lele, Script. Metall. Mater. **29**, 1131 (1993).

[194]A. Letzel, B. Gökce, P. Wagener, S. Ibrahimkutty, A. Menzel, A. Plech and S. Barcikowski, J. Phys. Chem. C **121**, 5356 (2017).

[195]D. H. Everett, Basic principles of colloid science. Royal society of chemistry. (University of Bristol, 2007).

[196]S. Markutsya, Modeling and simulation of nanoparticle aggregation in colloidal systems. Retrospective Theses and Dissertations. 15299. Iowa State University Ames, Iowa, USA. (2010).

[197]E. Matijevic and. R. J. Good (Eds.) Surface and colloid science (Vol. 12). Springer Science & Business Media (2012).

[198]T. Cosgrove, Colloid science. (Blackwell publishing limited, 2005).

[199]M. Kolb, R. Botet and R. Jullien, Phys. Rev. Lett. **51**, 1123 (1983).

[200]P. Meakin, Phys. Rev. Lett. **51**, 1119 (1983).

[201]T. A. Witten Jr and L. M. Sander, Phys. Rev. Lett. **47**, 1400 (1981).

[202]M. Kolb, Phys. Rev. Lett. **53**, 1653 (1984).

[203]P. Meakin and F. Family, Phys. Rev. A **38**, 2110 (1988).

[204]B. Derjaguin and L.D. Landau, Acta Physicochimica U.R.S.S. **14**, 633 (1941)

[205]E. J. W. Verwey and J. T. G. Overbeek, J. Colloid Sci. **10**, 224 (1955).

[206]A. Ziashahabi, R. Poursalehi and N. Naseri, Mater. Sci. Semicond. Process. **72**, 128-133. (2017).

[207]S. Jungblut and A. Eychmüller, Modeling nanoparticle aggregation. Chemical Modelling: Volume 15, Editors: Michael Springborg, Jan-Ole Joswig, pp. 1-27 (2019).

[208]A. Ambrosetti, N. Ferri, R. A. DiStasio and A. Tkatchenko, Science **351**, 1171 (2016).

[209]H. Y. Kim, J. O. Sofo, D. Velegol, M. W. Cole and A. A. Lucas, J. Chem. Phys. **124**, 074504 (2006).

[210]Y. Xia, Y. Xiong, B. Lim and S. E. Skrabalak, Angewandte Chem. Int. Ed. **48**, 60 (2009).

[211]C. H. Lo, T. T. Tsung and L. C. Chen, J. Cryst. Growth **277**, 636 (2005).

[212]P. Lukes, B. R. Locke and J. L. Brisset, Plasma Chem. Catal. Gases Liquids **1**, 243 (2012).

[213]Z. Ke, Q. Huang, H. Zhang and Z. Yu, Environ. Sci. Technol. **45**, 7841 (2011).

[214]L. Wang and X. Jiang, Environ. Sci. Technol. **42**, 8492 (2008).

[215]S. H. Khezri, A. Yazdani and R. Khordad, Eur. Phys. J. Appl. Phys. **59**, 30401 (2012).

[216]S. H. Khezri, A. Yazdani, R. Khordad and B. A. Ravan, Modern Phys. Lett. B **27**, 1350057 (2013).

[217]D. J. Lee, S. J. Kim, J. Lee, H. Lee, H. G. Kim and S. C. Jung, Sci. Adv. Mater. **6**, 1599-1604 (2014).

[218]J.-Ph. Sylvestre, S. Poulin, A. V. Kabashin, E. Sacher, M. Meunier and J. H. T. Luong, J. Phys. Chem. B **108**, 16864 (2004).

[219]F. Mafuné, J. Y. Kohno, Y. Takeda, T. Kondow and H. Sawabe, J. Phys. Chem. B **104**, 8333 (2000).

[220]S. Dadashi, R. Poursalehi and H. Delavari, Procedia Mater. Sci. **11**, 722 (2015).

[221]M. C. Sportelli, M. Clemente, M. Izzi, A. Volpe, A. Ancona, R. A. Picca, G. Palazzo and N. Cioffi, Colloids Surf. A **559**, 148 (2018).

[222]M.-R. Kalus, R. Lanyumba, N. Lorenzo-Parodi, M. A. Jochmann, K. Kerpen, U. Hagemann, T. C. Schmidt, S. Barcikowski and B. Gökce, Phys. Chem. Chem. Phys. **21**, 18636 (2019).

[223]M. R. Kalus, V. Reimer, S. Barcikowski and B. Gökce, Discrimination of effects leading to gas formation during pulsed laser ablation in liquids. Appl. Surf. Sci. **465**, 1096 (2019).

[224]M. O. Fatehah, H. A. Aziz and S. Stoll, J. Colloid Sci. Biotechnol. **3**, 111 (2014).

[225]C. Shih, J. J. Molina and R. Yamamoto, Molec. Phys. **113**, 2511 (2015).

[226]C. T. O'Konski, J. Phys. Chem. **64**, 605 (1960).

[227]C. T. O'Konski, S. Krause, J. Phys. Chem. **74**, 3243 (1970).

[228]R. Li, Y. Wu and J. Xiao, J. Chem. Phys. **140**, 034503 (2014)

[229]B. J. Wiley, S. H. Im, Z. Y. Li, J. McLellan, A. Siekkinen and Y. Xia, J. Phys. Chem. B **110**, 15666 (2006).

[230]J. P. Kottmann, O. J. Martin, D. R. Smith and S. Schultz, Phys. Rev. B **64**, 235402 (2001).

[231]M. Muniz-Miranda, T. Del Rosso, E. Giorgetti, G. Margheri, G. Ghini, and S. Cicchi, Anal. Bioanal. Chem. **400**, 361 (2011).

[232]M. M. Isikawa, A. C. A. Assuncao, O. Baffa and E.J. Guidelli, J. Lumin. **231**, 117841 (2021).

[233]A. I. Henry, J. M. Bingham, E. Ringe, L. D. Marks, G. C. Schatz and R. P. Van Duyne, J. Phys. Chem. C **115**, 9291 (2011).

[234]A. A. Bonyár, I. Csarnovics, M. Veres, L. Himics, A. Csik, J. Kámán, L. Balázs and S. Kökényesi, S. Sens. Actuator B: Chem. **255**, 433 (2018)

[235]J. F. Li, C. Y. Li and R. F. Aroca, Chem. Soc. Rev. **46**, 3962 (2017).

[236]D. Gebauer, M. Kellermeier, J. D. Gale, L. Bergström and H. Cölfen, Chem. Soc. Rev. **43**, 2348 (2014).

[237]V. Germain, J. Li, D. Ingert, Z. L. Wang and M. P. Pileni, J. Phys. Chem. B **107**, 8717 (2003).

[238]H. Kabbara, J. Ghanbaja, A. Redjaïmia and T. Belmonte, J. Appl. Cryst. **52**, 304 (2019).

[239]K. Gouriet, M. Sentis and T. E. Itina, J. Phys. Chem. C **113**, 18462 (2009).

[240]S. P. Cho, M. A. Bratescu, N. Saito and O. Takai, Nanotechnol. **22**, 455701 (2011).

[241]S. H. Sun and S. C. Jung, Korean J. Chem. Eng. **33**, 1075 (2016).

[242]F. Font and T. G. Myers, J. Nanopart. Res. **15**, 2086 (2013).

[243]A. van Teijlingen, S. A. Davis and S. R. Hall, Nanoscale Adv. **2**, 2347 (2020).

[244]J. R. Sambles, L. M. Skinner and N. D. Lisgarten, Proc. Royal Soc. London. A. Math. Phys. Sci. **318**, 507 (1970).

[245]J. R. Sambles, Proc. Royal Soc. London. A. Math. Phys. Sci. **324**, 339 (1971).

[246]P. Grammatikopoulos, M. Sowwan and J. Kioseoglou, Adv. Theory Simul. **2**, 1900013 (2019).

[247]C. R. Stoldt, C. J. Jenks, P. A. Thiel, A. M. Cadilhe and J. W. Evans, J. Chem. Phys. **111**, 5157 (1999).

[248]K. E. Lehtinen and M. R. Zachariah, J. Aerosol Sci. **33**, 357 (2002).

[249]P. Grammatikopoulos, C. Cassidy, V. Singh and M. Sowwan, Sci. Rep. **4**, 5779 (2014).

[250]R. S. Averback and H. L. Zhu, Phil. Mag. Lett. **73**, 27 (1996).

[251]L. J. Lewis, P. Jensen and. J. L. Barrat, Phys. Rev. B **56**, 2248 (1997).

[252]A. Atkinson, Rev. Modern Phys. **57**, 437 (1985).

[253]C. Wagner, Z. Physik. Chem. **21**, 25 (1933).

[254]N. F. M. N. Cabrera and N. F. Mott, Rep. Prog. Phys. **12**, 163 (1949).

[255]A. T. Fromhold Jr., Theory of metal oxidation Vol 2., Netherlands: North-Holland Publ Co. (1980).

[256]C. Holse, C. F. Elkjær, A. Nierhoff, J. Sehested, I. Chorkendorff, S. Helveg and J. H. Nielsen, J. Phys. Chem. C **119**, 2804 (2015).

[257]C. M. Wang, D. R. Baer, L. E. Thomas, J. E. Amonette, J. Antony, Y. Qiang and G. Duscher, J. Appl. Phys. **98**, 094308 (2005).

[258]M. Varón, I. Ojea-Jimenez, J. Arbiol, L. Balcells, B. Martínez and V. F. Puntes, Nanoscale **5**, 2429-2436 (2013).

[259]C. H. Chen, T. Yamaguchi, K. I. Sugawara and K. Koga, J. Phys. Chem. B **109**, 20669 (2005).

[260]D. Q. Yang, J. N. Gillet, M. Meunier and E. Sacher. J. Appl. Phys. **97**, 024303 (2005).

[261]A. T. Fromhold Jr, J. Phys. Chem. Solids **49**, 1159 (1988).

[262]S. M. Kim, Y. J. Lee, J. W. Kim and S. Y. Lee, Thin Solid Films **572**, 260-265 (2014).

[263]P. Pootawang, N. Saito, O. Takai and S. Y. Lee, Nanotechnol. **23**, 395602 (2012).

[264]S. H. Rahaghi, R. Poursalehi and R. Miresmaeili, Proc. Mater. Sci. **11**, 738-742 (2015).

[265]A. A. Tsukanov, A. S. Lozhkomoev, M. I. Lerner, I. Gotman, E. Y. Gutmanas and S. G. Psakhie, Phil. Mag. **99**, 1121 (2019).

[266]R. Sergiienko, E. Shibata, A. Zentaro, D. Shindo, T. Nakamura and G. Qin, Acta Mater. **55**, 3671 (2007).

[267]Z. Abdullaeva, E. Omurzak, C. Iwamoto, H. S. Ganapathy, S. Sulaimankulova, C. Liliang and T. Mashimo, Carbon **50**, 1776 (2012).

[268]B. Xu, J. Guo, X. Wang, X. Liu and H. Ichinose, Carbon **44**, 2631 (2006).

[269]D. Zhang, C. Zhang, J. Liu, Q. Chen, X. Zhu and C. Liang, ACS Appl. Nano Mater. **2**, 28 (2018).

[270]T. Del Rosso, N. A. Rey, T. Rosado, S. Landi, D. G. Larrude, E. C. Romani, F. L. Freire Junior, S. M. Quinteiro, M. Cremona, R. Q. Aucelio, G. Margheri and O. Pandoli, Nanotechnol. **27**, 255602 (2016).

[271]T. Del Rosso, S. R. W. Louro, F. L. Deepak, E. C. Romani, Q. Zaman, O. Pandoli, M. Cremona, F. L. Freire Junior, P. A. A. De Beule, T. De St. Pierre, R. Q. Aucelio, G. Mariotto, S. Gemini-Piperni, A. R. Ribeiro, S. M. Landi and A. Magalhães, Appl. Surf. Sci. **441**, 347 (2018).

[272]H. Kabbara, J. Ghanbaja, C. Noël and T. Belmonte, Nano-Struct. Nano-Objects **10**, 22-29 (2017).

[273]H. Kabbara, C. Noel, J. Ghanbaja, K. Hussein, D. Mariotti, V. Švrček and T. Belmonte, Sci. Rep. **5**, 1 (2015).

[274]A. Hamdan, C. Noel, J. Ghanbaja, S. Migot-Choux and T. Belmonte, Mater. Chem. Phys. **142**, 199 (2013).

[275]R. Sergiienko, S. Kim, E. Shibata and T. Nakamura, J. Nanopart. Res. **12**, 481 (2010).

[276]M. Mardanian, N. V. Tarasenko and A. A. Nevar, Braz. J. Phys. **44**, 240 (2014).

[277]Q. Zaman, J. Souza, O. Pandoli, K. Q. Costa, V. Dmitriev, D. Fulvio, M. Cremona, R. Q. Aucelio, G. Fontes and T. Del Rosso, Opt. Express **27**, 3200 (2019).

[278]P. Georgiev, A. Bojinova, B. Kostova, D. Momekova, T. Bjornholm and K. Balashev, Colloids Surf. A: Physicochem. Engin. Aspects **434**, 154 (2013).

[279]E. Tomaszewska, K. Soliwoda, K. Kadziola, B. Tkacz-Szczesna, G. Celichowski, M. Cichomski, W. Szmaja and J. Grobelny, J. Nanomater. **313081**, (2013).

[280]F. Giammanco, E. Giorgetti, P. Marsili and A. Giusti, J. Phys. Chem. C **114**, 3354 (2010).

[281]N. Tarasenka ,A. Nominé, A. Nevar, M. Nedelko, H. Kabbara, S. Bruyère, J. Ghanbaja, C. Noel, A. Krasilin, G. Zograf, V. Milichko, N. Kulachenkov, S. Makarov, T. Belmonte and N. Tarasenko, Phys. Rev. Appl. **13**, 014021 (2020)

[282]B. J. Garrison,; T. E. Itina, L. V. Zhigilei, Phys. Rev. E **68**, 041501 (2003).

[283]H. Huang and L. V. Zhigilei, J. Phys. Chem. C **125**, 13413 (2021).

[284]N. Sano, O. Kawanami, T. Charinpanitkul and W. Tanthapanichakoon, Thin Solid Films **516**, 6694 (2008).

[285]S. Reich, P. Schönfeld, P. Wagener, A. Letzel, S. Ibrahimkutty, B. Gökce, S. Barcikowski, S. Menzel, T. dos Santos Rolo and A. Plech, J. Colloid Interf. Sci. **489**, 106 (2017).

[286]S. Reich, A. Letzel, A. Menzel, N. Kretzschmar, B. Gökce, S. Barcikowski and A. Plech, Nanoscale, **11**, 6962 (2019).

[287]A. Letzel, B. Gökce, A. Menzel, A. Plech and S. Barcikowski, Appl. Surf. Sci. **435**, 743 (2018).

[288]S. Menon and M. Lal, Exp. Therm. Fluid Sci. **16**, 305 (1998).

[289]N. Sano, H. Wang, I. Alexandrou, M. Chhowalla, K. B. K Teo, G. A. J. Amaratunga and K. Iimura, J. Appl. Phys. **92**, 2783-2788 (2002).

[290]C. H. Chon, S. Paik, J. B. Tipton and K. D. Kihm, Langmuir **23**, 2953 (2007).

[291]U. Thiele, I. Vancea, A. J. Archer, M. J. Robbins, L. Frastia, A. Stannard, E. Pauliac-Vaujour, C. P. Martin, M. O. Blunt and P. J. Moriarty, J. Phys.: Cond. Matter **21**, 264016 (2009).

[292]R. H. Chen, T. X. Phuoc and D. Martello, Int. J. Heat Mass Transfer **53**, 3677 (2010).

[293]L. H. López, L. M. Monzonís, L. B. Vicente, J. Kaur and M. H. Buschman (Eds.), Report about nanofluid's health, safety and environmental impact. Int. J. Therm. Sci, 129, 504-531 (2018).

[294]S. U. Choi, J. Heat Transfer **131**, 033106 (2009).

[295]D. Mariotti, V. Švrček, J. W. Hamilton, M. Schmidt and M. Kondo, Adv. Funct. Mater. **22**, 954 (2012).

[296]V. Burakov, V. Kiris, M. Nedelko, N. Tarasenka, A. Nevar and N. Tarasenko, J. Phys. D: Appl. Phys. **51**, 484001 (2018).

[297]D. Mariotti, S. Mitra and V. Švrček, Nanoscale **5**, 1385 (2013).

[298]N. G. Loucaides, A. Ramos and G. E. Georghiou, J. Phys.: Conf. Series **100**, 052015 (2008).

[299]W. Hilber, B. Weiss, M. Mikolasek, R. Holly, K. Hingerl and B. Jakoby, J. Micromech. Microeng. **18**, 064016 (2008).

[300]B. C. Gierhart, D. G. Howitt, S. J. Chen, R. L. Smith and S. D. Collins, Langmuir **23**, 12450 (2007).

[301]A. Ramos, P. García-Sánchez and H. Morgan, Curr. Opin. Colloid Interf. Science **24**, 79 (2016).

[302]S. O. Lumsdon and D. M. Scott, Langmuir **21**, 4874 (2005).

[303]L. Bernard, M. Calame, S. J. Van Der Molen, J. Liao and C. Schönenberger, Nanotechnol. **18**, 235202 (2007).

[304]K. D. Hermanson, S. O. Lumsdon, J. P. Williams, E. W. Kaler and O. D. Velev, Science **294**, 1082 (2001).

[305]R. J. Barsotti Jr, M.D. Vahey, R. Wartena, Y. M. Chiang, J. Voldman and F. Stellacci, Small **3**, 488 (2007).

[306]M. Washizu and T. B. Jones, J. Electrostat. **38**, 199 (1996).

[307]V. N. Shilov and T. S. Simonova, Colloid J. USSR **43**, 90 (1981).

[308]K. Y. Leong, R. Saidur, S. N. Kazi and A. H. Mamun Appl. Therm. Eng. **30**, 2685-2692 (2010).

[309]S. Toghyani, E. Afshari, E. Baniasadi and M. S. Shadloo, Renew. Energy **141**, 1013 (2019).

[310]S. K. Choi, H.A. Son, H. T. Kim and J. W. Kim, Energy Fuels, **31**, 7777 (2017).

[311]R. Jalal, E. K. Goharshadi, M. Abareshi, M. Moosavi, A. Yousefi and P. Nancarrow, Mater. Chem. Phys. **121**, 198 (2010).

[312]F. Tamaddon, F. Aboee and A. Nasiri, Catal. Comm. **16**, 194 (2011).

[313]V. Mahendran and J. Philip, Appl. Phys. Lett. **100**, 073104 (2012).

[314]Z. Swiatkowska-Warkocka, K. Koga, K. Kawaguchi, H. Wang, A. Pyatenko and N. Koshizaki, RSC Adv. **3**, 79 (2013).

[315]Z. Swiatkowska-Warkocka, A. Pyatenko, F. Krok, B. R. Jany and M. Marszalek, Sci. Rep. **5**, 9849 (2015).

[316]L. Yang, L. Chen, Y. C. Chen, L. Kang, J. Yu, Y. Wang, C. Lu, T. Mashimo, A. Yoshiasa and C. H. Lin, Colloids Surf. B: Biointerf. **180**, 466 (2019).

[317]A. O. Larin, A. Nominé, E. I. Ageev, J. Ghanbaja, L. N. Kolotova, S. V. Starikov, S. Bruyère, T. Belmonte, S. V. Makarov and D. A. Zuev, Nanoscale **12**, 1013 (2020).

[318]F. Cataldo, Tetrahedron **60**, 4265 (2004).

[319]J. Senthilnathan, C. C. Weng, J. D. Liao and M. Yoshimura, Sci. Rep. **3**, 2414 (2013).

[320]F. Oshima, S. Stauss, C. Ishii, D. Z. Pai and K. Terashima, J. Phys. D: Appl. Phys. **45**, 402003 (2012).

[321]P. Lukes, E. Dolezalova, I. Sisrova and M. Clupek, Plasma Sources Sci. Technol. **23**, 015019 (2014).

[322]G. Ahmed, M. Hanif, L. Zhao, M. Hussain, J. Khan and Z. Liu, J. Molec. Catal. A: Chem. **425**, 310 (2016).

[323]J. Ortiz-Medina, Z. Wang, R. Cruz-Silva, A. Morelos-Gomez, F. Wang, X. Yao, M. Terrones and M. Endo, Adv. Mater. **31**, 1805717 (2019).

Liquid (Volume)	I(A)	V_{appl} (V)	T_{on} (µs)	T_{off} (µs)	Gap (µm)	Gap control	Particles*	Electrodes**	Comments	Ref.
Liquid nitrogen	70	DC: 10000	0.1–2.5	3.3×10^5	100	Hand	Ag NPs, Cd NCs and NWs Ag: (30-50 nm) Cd: (5-10 nm)	2: Ag or 2: Cd	Self-assembly of Cd NCs into NWs	127
Deionized Water (200 mL)	11.5	DC: 140	5–1000	1000–5	30	Servo	Ag or AgO (1– 200 nm) NPs Trimodal (1,5 / 6 / 80 nm)	2: Ag	Cathode is twice larger than anode	128
Distilled water	50–150	DC: 27			1000	Yes	Oxidized Al, Cu and Al–Cu composite NPs and MPs	2: Al or 2: Cu or 1:Al + 1 Cu	1 Al electrode and 1 Cu electrode	129
Liquid ammonia at 100°C and n-heptane at 25°C	Current frequency: 1–2 Hz	DC: 11000 for NH_3 DC: 7500 for heptane			No gap	-	AlN, TiN, Fe, Cr_2N in NH_3 Al_4C_3, TiC, Fe, Fe_2C and Cr_7C_3 in heptane. (1–10 µm)	2: Al (for AlN and Al_4C_3) or 2: Ti	Pellets of Al, Ti, Fe and Cr as starting material and put between 2 eletrodes	36
$HAuCl_4$ solution	15	DC: 3			Adjusted to set current	Hand	Au NPs (8 ± 3 nm)	2: Ti	Electrode in contact for ignition	130, 131
0.01 M $HAuCl_4$-xH_2O		DC: -1000	0.02			Single electrode	Au NPs Unimodal (36 ± 9 nm)	200 nm carbon nanopipettes	Single pulse applied	132
100 mL deionized water or pure ethanol	2-12	DC: 3200	1	999	unknown	1 movable electrode	Au NPs Unimodal (20 ± 15 nm)	2: Au wires	Ultrasound assistance	133
$HAuCl_4$-$3H_2O$ (0.5mM), distilled water (200 ml) + 2.0mM KOH		DC: 2000			500		Au NPs Unimodal (23 ± 9 nm)	2: W wires		134
$HAuCl_4$-$4H_2O$ (37mM) + Sodium dodecyl sulfonate (0.01 mol) added to 150 ml of water		DC: 1600 and 3200	2	64.6	300	Constant	Au NPs with exotic shape Unimodal (25-50 nm) and (10-20 nm)	2: W wires	Utilization of SDS as surfactant	135
Deionized water	4	DC: 70–100V (2–3µs)	10	50	A few µm	Servo	Au NPs Unimodal (15-30 nm)	2:Au wires		136, 137

		and 20–40V pulse								
Hexane	Unknown	Single pulse (0.05 J)	Unknown	Unknown	Unknown	Unknown	Fusiform Au NPs after reduction with sodium citrate from Au nano-dispersion L: 50-150 nm D: 5 to 15 nm	2: Au (V-shape configuration)	Post-treatment: exposed to aqua regia for 20 min and next 1% sodium citrate dispersion.	138
Ethanol	6.4	DC: 135V and 18V after breakdown	50	50	20-40	Servo	Au NPs Unimodal (8 ± 6 nm)	2: Au		139
Liquid nitrogen	~100	DC: 10000	0.1	10^5	100	Hand	Cu, Ag, Cu_xAg_y alloys Trimodal (2-10 nm / 30-50 nm / large)	2: Cu or 2: Ag or 2: $Cu_{28}Ag_{72}$	x < 8.8 wt% or x > 92wt%	140
Liquid nitrogen	~100	DC: 10000	0.075	10^5	100	Hand	Cu NPs, Zn NPs and NSs, Cu@Zn NPs Trimodal (2-10 nm / 30-50 nm / large)	2: Cu or 2: Ag or 1: Cu + 1:Zn	Cu NPs are wrapped in Zn NSs.	141
Water + 0.007 wt% NaCl	Unknown	DC: Unknown (High Voltage)	1–2	99–98	300–500	Hand	Fibre-shaped (CuO) NPs and flower-shaped ZnO NPs Bimodal (15–25 / 50–60 nm)	2: Cu or 2 : Zn		142
Deionized Water (150 mL)	0.5–25	DC: 90–220	2–2400	2400–2		Servo	CuO NPs (20–200 nm) (68 nm ± 33 nm)	2: Cu	Fluid cooled between 2 and 25°C. Pressure [20–760 Torr]	143
5 mM $CuCl_2$, 10 mM ascorbic acid in 1% by weight gelatin solution (130 ml deionized water).	0.002	DC: 900	12.5–35	15–37.5	500	Constant	Cu NPs (around 25 nm) with shape changing vs treatment time. sphere/ cube / hexagon / triangle (33.7 ± 5.8 nm) / (19.2 ± 3.3 nm) / (20.3 ± 2.9 nm) / (35.1 ± 7.6 nm)	2: W		144

0.1 mol/L $NaNO_3$ solution		AC: 150					CuO colloidal reduced chemically to Cu_2O and Cu NRs After 30 min (1-2 nm)	2: Cu	Chemical reduction: 0.1 mol/L ascorbic acid and 1 mL hydrazine hydrate (35 wt%)	145
Deionized Water (0.5 L)	1.5	DC: 220	12	2	7	Servo (current)	TiO_2 NPs (a few 100s of nm) Unimodal (80 nm)	2: Ti		146
Deionized Water (3 L)	50	DC: 28–34	-	-	1000	Hand	$Cd(OH)_2$ NPs and NWs D: 5–40 nm	2: Cd	NWs formed by NPs assembly	147
Liquid nitrogen	30	DC: 10000	0.3	3.3×10^5	100	Hand	PbO_2 NSs D=several µm	2: Pb		148
Ethyl alcohol (60 mL)	120	DC: 0, 300, 500	20	9980	Unknown	No	W, Ni, C, Steel NPs and MPs D: 15–20 nm	2: W, Ni, C or Steel		149
Liquid nitrogen	70	DC: 8000–12000	0.1–2.5	3.3×10^5	100	Hand	Co, Ni, CoNi alloy NPs Trimodal (4-15 nm / 30-60 nm / large)	2: Co or 2: Ni or 1: Co + 1:Ni		150

* NPs: Nanoparticles – MPs: Microparticles – NWs: Nanowires – NSs: Nanosheets –NCs: Nanocubes – NRs: Nanorods

** 0, 1+1 or 2 means no electrode, 1 electrode made of a given material and 1 electrode made of another material or 2 electrodes made of the same materials.

Table 1: Submerged discharges in liquids used to synthesize nano-objects.